PHYSICAL REVIEW D **88,** 074017 (2013)

Comparing symmetry restoration trends for meson masses and mixing angles in the QCD-like three quark flavor models

Vivek Kumar Tiwari*

Department of Physics, University of Allahabad, Allahabad 211002, India

(Received 15 January 2013; published 14 October 2013)

We are computing the modifications for the scalar and pseudoscalar meson masses and mixing angles due to the proper accounting of fermionic vacuum fluctuation in the framework of the generalized 2 + 1 flavor quark meson model and the Polyakov loop augmented quark meson model (PQM). The renormalized contribution of the divergent fermionic vacuum fluctuation at one loop level makes these models effective QCD-like models. It has been explicitly shown that analytical expressions for the model parameters, meson masses, and mixing angles do not depend on any arbitrary renormalization scale. We have investigated how the incorporation of fermionic vacuum fluctuation in quark meson and PQM models qualitatively and quantitatively affects the convergence in the masses of the chiral partners in pseudoscalar (π, η, η', K) and scalar (σ, a_0, f_0, κ) meson nonets as the temperature is varied on the reduced temperature scale. Comparison of present results in the quark meson model with vacuum term and the PQM model with vacuum term with the already existing calculations in the bare 2 + 1 quark meson and PQM models shows that the restoration of chiral symmetry becomes smoother due to the influence of the fermionic vacuum term. We find that the melting of the strange condensate registers a significant increase in the presence of the fermionic vacuum term and its highest melting is found in the PQM model with vacuum term. The role of the $U_A(1)$ anomaly in determining the isoscalar masses and mixing angles for the pseudoscalar (η and η') and scalar (σ and f_0) meson complex has also been significantly modified due to the fermionic vacuum correction. In its influence, the interplay of chiral symmetry restoration and the setting up of the $U_A(1)$ restoration trends have also been shown to be significantly modified.

DOI: 10.1103/PhysRevD.88.074017 PACS numbers: 12.38.Aw, 11.10.Wx, 11.30.Rd, 12.39.Fe

I. INTRODUCTION

The strong interaction theory predicts that normal hadronic matter goes through a phase transition and produces a collective form of matter known as the quark gluon plasma (QGP) under the extreme conditions of high temperature and/or density when the individual hadrons dissolve into their quark and gluon constituents [1–6]. Relativistic heavy ion collision experiments at RHIC (BNL) and LHC (CERN) and the future CBM experiments at the FAIR facility (GSI-Darmstadt) aim to create and study such a collective state of matter. Study of the different aspects of this phase transition is a tough and challenging task because QCD, which is the theory of strong interaction, becomes nonperturbative in the low-energy limit. However, the QCD vacuum reveals itself through the process of spontaneous chiral symmetry breaking and the phenomenon of color confinement.

In the zero quark mass limit, the chiral condensate works as an order parameter for the spontaneous breakdown of the chiral symmetry in the low-energy hadronic vacuum of QCD. For the infinitely heavy quarks, in the pure gauge $SU_c(3)$ QCD, the $Z(3)$ [center symmetry of the QCD color gauge group] symmetry, which is the symmetry of the hadronic vacuum, gets spontaneously broken in the high temperature/density regime of QGP. Here the expectation value of the Wilson line (Polyakov loop) is related to the free energy of a static color charge; hence, it serves as the order parameter of the confinement-deconfinement phase transition [7]. Even though the center symmetry is always broken with the inclusion of dynamical quarks in the system, one can regard the Polyakov loop as an approximate order parameter because it is a good indicator of the confinement-deconfinement transition [8,9].

The lattice QCD calculations (see e.g., [10–25]) give us important information and insights regarding various aspects of the transition, like the restoration of chiral symmetry in QCD, order of the confinement-deconfinement phase transition, richness of the QCD phase structure, and mapping of the phase diagram. Since lattice calculations are technically involved and various issues are not conclusively settled within the lattice community, one resorts to the calculations within the ambit of phenomenological models [26–41] developed in terms of effective degrees of freedom. These model investigations complement the lattice simulation studies and give much needed insight about the regions of phase diagram inaccessible to lattice simulations. Lot of current effective model-building activity is centered around combining the features of spontaneous breakdown of both chiral symmetry and the center $Z(3)$ symmetry of QCD in one single model (see for example [42–69]). In these models, the chiral condensate and Polyakov loop are simultaneously coupled to the quark degrees of freedom.

*vivekkrt@gmail.com

The behavior patterns of mesons and their properties in the hot and dense medium have been investigated in several two- and three-flavor Nambu-Jona-Lasinio (NJL), Polyakov-Nambu-Jona-Lasinio (PNJL) models (e.g., [70–75]) and also in the $SU(2)$ version of linear sigma model (e.g., [28,30,34]). Since the parity doubling of mesons signals the restoration of chiral symmetry, these studies look for the emergence of mass convergence patterns in the masses of the chiral partners in pseudoscalar (π, η, η', K) and scalar mesons (σ, a_0, f_0, κ). We know that the basic QCD Lagrangian has the global $SU_{R+L}(3) \times SU_{R-L}(3) \times U_A(1)$ symmetry. For the $SU(3)$ linear sigma model, several explicit as well as spontaneous symmetry-breaking patterns of $SU_V(3) \times SU_A(3)$ have been discussed by Lenaghan *et al.* in Ref. [29]. Enlarging the linear sigma model with the inclusion of quarks [35] in the 2 + 1 flavor-breaking scenario, Schaefer *et al.* studied the consequences of $SU(3)$ chiral symmetry restoration for scalar and pseudoscalar meson masses and mixing angles in the presence as well as the absence of $U_A(1)$ axial symmetry, as the temperature is increased through the phase transition temperature. It was shown by 't Hooft [76] that the $U_A(1)$ axial symmetry does not exist at the quantum level, and the instanton effects explicitly break it to $Z_A(N_f)$. Due to the $U_A(1)$ anomaly, the η' meson does not remain a massless Goldstone boson in the chiral limit of zero quark masses, and it acquires a mass of about 1 GeV. This happens due to the flavor mixing, a phenomenon that lifts the degeneracy between the π and η', which otherwise would have been degenerate with π in $U(3)$ even if the explicit chiral symmetry breaking is present. There is large violation in the Okubo-Zweig-Iizuka (OZI) rule for both pseudoscalar and scalar mesons, and ideal mixing is not achieved because of strong flavor mixing between nonstrange and strange flavor components of the mesons [73]. Hence, $U_A(1)$ restoration will have important observable effects on scalar and pseudoscalar meson masses as well as on the mixing angles.

The effect of the Polyakov loop potential on the behavior of meson masses and mixing angles has been studied by Costa *et al.* in the PNJL model [73] and by Contrera *et al.* in the nonlocal PNJL model [74]. Here, in the NJL model–based studies, mesons are generated by some prescription [72] and the η' is not a well-defined quantity [77]. It becomes unbound soon after the temperature is raised from zero. In the 2 + 1 flavor quark meson linear sigma model investigations by Schaefer *et al.* [35,36], the mesons are the explicit degrees of freedom included in the Lagrangian from the very outset and the $U_A(1)$-breaking 't Hooft coupling term is constant. Recently, we investigated the influence of the Polyakov loop potential on the meson mass and mixing angle variations in the scalar and pseudoscalar sector, in the framework of the generalized 2 + 1 flavor quark meson model enlarged with the inclusion of the Polyakov loop [44–47].

The chiral symmetry-breaking mechanism in the Quark-Meson/Polyakov-Quark-Meson (QM/PQM) model is different from that of the NJL/PNJL model. In the NJL/PNJL model, the fermionic vacuum fluctuation leads to the dynamical breaking of the chiral symmetry while in most of the QM/PQM model calculations, the fermionic vacuum loop contribution to the grand potential has frequently been neglected until recently [30,34–37,51], because here the spontaneous breaking of chiral symmetry is generated by the mesonic potential itself. Recently, Skokov *et al.* incorporated the appropriately renormalized fermionic vacuum fluctuation [78] in the thermodynamic potential of the two-flavor QM model, which becomes an effective QCD-like model because now it can reproduce the second-order chiral phase transition at $\mu = 0$ as expected from the universality arguments [26] for the two massless flavors of QCD. The fermionic vacuum correction and its influence have also been investigated in earlier works [79–82]. In a recent work [83], we generalized the proper accounting of renormalized fermionic vacuum fluctuation in the two-flavor PQM model to the nonzero chemical potentials and found that the position of critical end point shifts to a significantly higher chemical potential in the μ and T plane of the phase diagram. Very recently, Schaefer *et al.* [84] estimated the size of the critical region around the critical end point in a three-flavor PQM model in the presence of the fermionic vacuum term. Sandeep *et al.* also investigated the phase structure and made comparisons with lattice data in another recent 2 + 1 quark flavor study with the effect of the fermionic vacuum term [85]. In a very recent work [86], the present author explored and compared the details of criticality in the two-flavor QM, PQM models in the presence and absence of fermionic vacuum correction.

In the present work, the author will explore how the proper accounting of fermionic vacuum correction in the QM and PQM models qualitatively and quantitatively affects the convergence of the masses of chiral partners when the parity doubling takes place as the temperature is increased through T_c and the partial restoration of chiral symmetry is achieved. We will also be studying the effect of fermionic vacuum correction on the interplay of $SU_A(3)$ chiral symmetry and $U_A(1)$ symmetry restoration in the presence as well as absence of Polyakov loop potential in the QM model.

The arrangement of this paper is as follows. In Sec. II, we recapitulate the model formulation. The grand potential in the mean-field approach has been described in Sec. III, where the subsection III A explicitly explains the procedure for obtaining the scale-independent expression of the effective potential after renormalizing the one-loop fermionic vacuum fluctuation. The numerical values of the model parameters are also given in this subsection, while the mathematical details for determining the renormalization scale independent parameters are given in Appendix A. The final expressions of the renormalization scale independent vacuum meson masses are derived in Appendix B. The Section IV gives the model formulas of meson masses and

mixing angles in a finite temperature/density medium. In Sec. V, we discuss the numerical results and plots for understanding and analyzing the effect of fermionic vacuum correction on chiral symmetry restoration. The summary and conclusion are presented in Sec. VI.

II. MODEL FORMULATION

We will be working in the generalized three-flavor quark meson chiral linear sigma model, which has been combined with the Polyakov loop potential [44–47]. In this model, quarks coming in three flavors are coupled to the $SU_V(3) \times SU_A(3)$ symmetric mesonic fields together with a spatially constant temporal gauge field represented by the Polyakov loop potential. The Polyakov loop field Φ is defined as the thermal expectation value of color trace of the Wilson loop in temporal direction,

$$\Phi = \frac{1}{N_c}\langle \mathrm{Tr}_c L(\vec{x})\rangle, \qquad \Phi^* = \frac{1}{N_c}\langle \mathrm{Tr}_c L^\dagger(\vec{x})\rangle, \tag{1}$$

where $L(\vec{x})$ is a matrix in the fundamental representation of the $SU_c(3)$ color gauge group,

$$L(\vec{x}) = \mathcal{P}\exp\left[i\int_0^\beta d\tau A_0(\vec{x},\tau)\right]. \tag{2}$$

Here $\mathcal{P}$ is path ordering, A_0 is the temporal vector field, and $\beta = T^{-1}$ [7].

The model Lagrangian is written in terms of quarks, mesons, couplings, and Polyakov loop potential $\mathcal{U}(\Phi, \Phi^*, T)$,

$$\mathcal{L}_{\mathrm{PQM}} = \mathcal{L}_{\mathrm{QM}} - \mathcal{U}(\Phi, \Phi^*, T), \tag{3}$$

where the Lagrangian in the quark meson chiral sigma model is

$$\mathcal{L}_{\mathrm{QM}} = \bar{q}_f(i\gamma^\mu D_\mu - gT_a(\sigma_a + i\gamma_5\pi_a))q_f + \mathcal{L}_m. \tag{4}$$

The coupling of quarks with the uniform temporal background gauge field is effected by the following replacement: $D_\mu = \partial_\mu - iA_\mu$ and $A_\mu = \delta_{\mu 0}A_0$ (Polyakov gauge), where $A_\mu = g_s A^a_\mu \lambda^a/2$ with vector potential A^a_μ for the color gauge field. g_s is the $SU_c(3)$ gauge coupling. λ_a are Gell-Mann matrices in the color space, a runs from $1 \ldots 8$. $q_f = (u, d, s)^T$ denotes the quarks coming in three flavors and three colors. T_a represents 9 generators of $U(3)$-flavor symmetry with $T_a = \frac{\lambda_a}{2}$ and $a = 0, 1 \ldots 8$; here, λ_a are standard Gell-Mann matrices in flavor space with $\lambda_0 = \sqrt{\frac{2}{3}}\mathbf{1}$. g is the flavor blind Yukawa coupling that couples the three flavors of quarks with nine mesons in the scalar (σ_a, $J^P = 0^+$) and pseudoscalar (π_a, $J^P = 0^-$) sectors.

The quarks have no intrinsic mass but become massive after spontaneous chiral symmetry breaking because of the nonvanishing vacuum expectation value of the chiral condensate. The mesonic part of the Lagrangian has the following form:

$$\begin{aligned}\mathcal{L}_m = {} & \mathrm{Tr}(\partial_\mu M^\dagger \partial^\mu M) - m^2\mathrm{Tr}(M^\dagger M) - \lambda_1[\mathrm{Tr}(M^\dagger M)]^2 \\ & - \lambda_2\mathrm{Tr}(M^\dagger M)^2 + c[\det(M) + \det(M^\dagger)] \\ & + \mathrm{Tr}[H(M + M^\dagger)].\end{aligned} \tag{5}$$

The chiral field M is a 3×3 complex matrix comprised of the nine scalars σ_a and the nine pseudoscalar π_a mesons,

$$M = T_a\xi_a = T_a(\sigma_a + i\pi_a). \tag{6}$$

The generators follow $U(3)$ algebra, $[T_a, T_b] = if_{abc}T_c$ and $\{T_a, T_b\} = d_{abc}T_c$ where f_{abc} and d_{abc} are standard antisymmetric and symmetric structure constants, respectively, with $f_{ab0} = 0$ and $d_{ab0} = \sqrt{\frac{2}{3}}\mathbf{1}\delta_{ab}$ and matrices normalized as $\mathrm{Tr}(T_aT_b) = \frac{\delta_{ab}}{2}$.

The $SU_L(3) \times SU_R(3)$ chiral symmetry is explicitly broken by the explicit symmetry-breaking term,

$$H = T_a h_a. \tag{7}$$

Here, H is a 3×3 matrix with nine external parameters. The ξ field that denotes both the scalar and pseudoscalar mesons picks up the nonzero vacuum expectation value, $\bar{\xi}$, for the scalar mesons due to the spontaneous breakdown of the chiral symmetry, while the pseudoscalar mesons have zero vacuum expectation value. Since $\bar{\xi}$ must have the quantum numbers of the vacuum, explicit breakdown of the chiral symmetry is only possible with the following three nonzero parameters: h_0, h_3, and h_8. We are neglecting isospin symmetry breaking; hence, we choose $h_0, h_8 \neq 0$. This leads to the $2 + 1$ flavor symmetry-breaking scenario with nonzero condensates $\bar{\sigma}_0$ and $\bar{\sigma}_8$.

Apart from h_0 and h_8, the other parameters in the model are five in number. These are the squared tree-level mass of the meson fields m^2, quartic coupling constants λ_1 and λ_2, a Yukawa coupling g, and a cubic coupling constant c, which models the $U_A(1)$ axial anomaly of the QCD vacuum.

Since it is broken by the quantum effects, the $U_A(1)$ axial, which otherwise is a symmetry of the classical Lagrangian, becomes anomalous [87] and gives large mass to the η' meson ($m_{\eta'} = 940$ MeV). In the absence of the $U_A(1)$ anomaly, the η' meson would have been the ninth pseudoscalar Goldstone boson, resulting from the spontaneous breakdown of the chiral $U_A(3)$ symmetry. The entire pseudoscalar nonet corresponding to the spontaneously broken $U_A(3)$ would consist of the three π, four K, and η and η' mesons, which are the massless pure Goldstone modes when $H = 0$. They become pseudo-Goldstone modes after acquiring finite mass due to nonzero H in different symmetry-breaking scenarios. The particles coming from octet (a_0, f_0, κ) and singlet (σ) representations of the $SU_V(3)$ group constitute a scalar nonet (σ, a_0, f_0, κ). In order to study the chiral symmetry restoration at high temperatures, we will be investigating the trend of convergence in the masses of chiral partners occurring in

pseudoscalar (π, η, η', K) and scalar (σ, a_0, f_0, κ) nonets, in the 2 + 1 flavor symmetry-breaking scenario.

A. Polyakov loop potential

The effective potential $\mathcal{U}(\Phi, \Phi^*, T)$ is constructed such that it reproduces the thermodynamics of pure glue theory on the lattice for temperatures upto about twice the deconfinement phase transition temperature. In this work, we are using logarithmic form of Polyakov loop effective potential [54]. The results produced by this potential are known to be fitted well to the lattice results. This potential is given by the following expression,

$$\frac{\mathcal{U}_{\log}(\Phi, \Phi^*, T)}{T^4} = -\frac{a(T)}{2}\Phi^*\Phi + b(T)\ln[1 - 6\Phi^*\Phi + 4(\Phi^{*3} + \Phi^3) - 3(\Phi^*\Phi)^2], \quad (8)$$

where the temperature-dependent coefficients are as follows:

$$a(T) = a_0 + a_1\left(\frac{T_0}{T}\right) + a_2\left(\frac{T_0}{T}\right)^2 \qquad b(T) = b_3\left(\frac{T_0}{T}\right)^3.$$

The parameters of Eq. (8) are

$$a_0 = 3.51, \quad a_1 = -2.47, \quad a_2 = 15.2, \quad b_3 = -1.75.$$

The critical temperature for the deconfinement phase transition $T_0 = 270$ MeV is fixed for the pure gauge Yang Mills theory. In the presence of dynamical quarks, T_0 is directly linked to the mass-scale Λ, the parameter which has a flavor and chemical potential dependence in full dynamical QCD and $T_0 \to T_0(N_f, \mu)$. The N_f and μ dependence of T_0 [42,43,48,49,84] is written as

$$T_0(N_f, \mu) = T_\tau e^{-1/(\alpha_0 b(N_f, \mu))}, \quad (9)$$

where $T_\tau = 1.77$ GeV denotes the τ scale and $\alpha_0 = \alpha(\Lambda)$ the gauge coupling at some UV scale Λ. The μ-dependent running coupling reads

$$b(N_f, \mu) = b(N_f) - b_\mu \frac{\mu^2}{T_\tau^2}, \quad (10)$$

the factor $b_\mu \simeq \frac{16}{\pi} N_f$. References [42,48] contain the details of the formula. Our present computations have been done at $\mu = 0$ and further since the N_f dependence of T_0 has additional complications of systematic error [48], we have taken $T_0 = 270$ MeV in our calculation as in Ref. [84].

III. GRAND POTENTIAL IN THE MEAN-FIELD APPROACH

We are considering a spatially uniform system in thermal equilibrium at finite temperature T and quark chemical potential μ_f ($f = u$, d and s). The partition function is written as the path integral over quark/antiquark and meson fields [35,44],

$$\mathcal{Z} = \mathrm{Tr}\exp\left[-\beta\left(\hat{\mathcal{H}} - \sum_{f=u,d,s}\mu_f\hat{\mathcal{N}}_f\right)\right] = \int\prod_a \mathcal{D}\sigma_a\mathcal{D}\pi_a\int\mathcal{D}q\mathcal{D}\bar{q}\exp\left[-\int_0^\beta d\tau\int_V d^3x\left(\mathcal{L}^{\mathcal{E}}_{\mathcal{QM}} + \sum_{f=u,d,s}\mu_f\bar{q}_f\gamma^0 q_f\right)\right], \quad (11)$$

where V is the three-dimensional volume of the system, $\beta = \frac{1}{T}$, and the superscript $\mathcal{E}$ denotes the Euclidean Lagrangian. For three quark flavors, in general, the three quark chemical potentials are different. In this paper, we assume that $SU_V(2)$ symmetry is preserved and neglect the small difference in masses of u and d quarks. Thus the quark chemical potential for the u and d quarks becomes equal, $\mu_x = \mu_u = \mu_d$. The strange quark chemical potential is $\mu_y = \mu_s$. Further, we consider symmetric quark matter and net baryon number to be zero.

Here, the partition function is evaluated in the mean-field approximation [30,35,36,44]. We replace meson fields by their expectation values, $\langle M\rangle = T_0\bar{\sigma}_0 + T_8\bar{\sigma}_8$, and neglect both thermal and quantum fluctuations of meson fields, while quarks and antiquarks are retained as quantum fields. Now, following the standard procedure as given in Refs. [42,53,63,88], one can obtain the expression of grand potential as the sum of pure gauge-field contribution, $\mathcal{U}(\Phi, \Phi^*, T)$, meson contribution, and quark/antiquark contribution evaluated in the presence of the Polyakov loop,

$$\Omega_{\mathrm{MF}}(T, \mu) = -\frac{T\ln Z}{V} = U(\sigma_x, \sigma_y) + \mathcal{U}(\Phi, \Phi^*, T) + \Omega_{\bar{q}q}(T, \mu). \quad (12)$$

The mesonic potential $U(\sigma_x, \sigma_y)$ is obtained from the $U(\sigma_0, \sigma_8)$ after transforming the original singlet-octet (0, 8) basis of condensates to the nonstrange-strange basis (x, y) as in Refs. [29,35,44,84]. We write the mesonic potential as

$$U(\sigma_x, \sigma_y) = \frac{m^2}{2}(\sigma_x^2 + \sigma_y^2) - h_x\sigma_x - h_y\sigma_y - \frac{c}{2\sqrt{2}}\sigma_x^2\sigma_y + \frac{\lambda_1}{2}\sigma_x^2\sigma_y^2 + \frac{1}{8}(2\lambda_1 + \lambda_2)\sigma_x^4 + \frac{1}{8}(2\lambda_1 + 2\lambda_2)\sigma_y^4, \quad (13)$$

where

$$\sigma_x = \sqrt{\frac{2}{3}}\bar{\sigma}_0 + \frac{1}{\sqrt{3}}\bar{\sigma}_8, \tag{14}$$

$$\sigma_y = \frac{1}{\sqrt{3}}\bar{\sigma}_0 - \sqrt{\frac{2}{3}}\bar{\sigma}_8. \tag{15}$$

The chiral symmetry-breaking external fields (h_x, h_y) are written in terms of (h_0, h_8) analogously.

Further, the nonstrange and strange quark/antiquark decouple, and the quark masses are

$$m_x = g\frac{\sigma_x}{2}, \qquad m_y = g\frac{\sigma_y}{\sqrt{2}}. \tag{16}$$

Quarks become massive in the symmetry-broken phase because of the nonzero vacuum expectation values of the condensates. The quark/antiquark contribution, in the presence of the Polyakov loop potential, is written as

$$\begin{aligned}\Omega_{\bar{q}q}(T,\mu) &= \Omega^{\rm vac}_{q\bar{q}} + \Omega^{\rm T}_{q\bar{q}} \\ &= -2\sum_{f=u,d,s}\int\frac{d^3p}{(2\pi)^3}[N_c E_f \theta(\Lambda^2 - \vec{p}^2) \\ &\quad + T\{\ln g_f^+ + \ln g_f^-\}].\end{aligned} \tag{17}$$

The first term of Eq. (17) represents the fermion vacuum one-loop contribution, regularized by the ultraviolet cutoff Λ. The expressions g_f^+ and g_f^- are defined in the second term after taking trace over the color space,

$$g_f^+ = [1 + 3\Phi e^{-E_f^+/T} + 3\Phi^* e^{-2E_f^+/T} + e^{-3E_f^+/T}], \tag{18}$$

$$g_f^- = [1 + 3\Phi^* e^{-E_f^-/T} + 3\Phi e^{-2E_f^-/T} + e^{-3E_f^-/T}], \tag{19}$$

$\mathrm{E}_f^{\pm} = E_f \mp \mu$, E_f is the flavor-dependent single particle energy of quark/antiquark, and m_f is the mass of the given quark flavor,

$$E_f = \sqrt{p^2 + m_f^2}. \tag{20}$$

A. Renormalization of the fermionic vacuum term and the effective potential

The first term of Eq. (17) can be properly renormalized using the dimensional regularization scheme, as done for the two-flavor case in Refs. [78,83,86] and the three-flavor case in Refs. [84,85]. The brief description of essential steps is given in the following. Fermion vacuum contribution is just the one-loop zero temperature effective potential at lowest order [89],

$$\begin{aligned}\Omega^{\rm vac}_{q\bar{q}} &= -2N_c\sum_{f=u,d,s}\int\frac{d^3p}{(2\pi)^3}E_f \\ &= -2N_c\sum_{f=u,d,s}\int\frac{d^4p}{(2\pi)^4}\ln(p_0^2 + E_f^2) + \mathrm{K}.\end{aligned} \tag{21}$$

K is the infinite constant independent of the fermion mass; hence, it is dropped. The dimensional regularization of Eq. (21) near three dimensions, $d = 3 - 2\epsilon$, gives the potential up to zeroth order in ϵ as

$$\Omega^{\rm vac}_{q\bar{q}} = \sum_{f=u,d,s}\frac{N_c m_f^4}{16\pi^2}\left[\frac{1}{\epsilon} - \frac{\{-3 + 2\gamma_E + 4\ln(\frac{m_f}{2\sqrt{\pi}\mathrm{M}})\}}{2}\right]. \tag{22}$$

Here M denotes the arbitrary renormalization scale. The addition of a following counterterm, $\delta\mathcal{L}$, to the QM/PQM model Lagrangian,

$$\delta\mathcal{L} = \sum_{f=u,d,s}\frac{N_c}{16\pi^2}m_f^4\left[\frac{1}{\epsilon} - \frac{1}{2}\{-3 + 2\gamma_E - 4\ln(2\sqrt{\pi})\}\right], \tag{23}$$

gives the renormalized fermion vacuum loop contribution as

$$\Omega^{\rm vac}_{q\bar{q}} = -\sum_{f=u,d,s}\frac{N_c}{8\pi^2}m_f^4\ln\left(\frac{m_f}{\mathrm{M}}\right). \tag{24}$$

We note that the Polyakov loop potential and the temperature-dependent part of the quark-antiquark contribution to the grand potential in Eq. (12) vanishes at $T = 0$ and $\mu = 0$. The Polyakov loop order parameter $\Phi = \Phi^*$ becomes zero in the low-temperature phase due to the phenomenon of color confinement, and this makes the Polyakov loop potential $\mathcal{U}_{\log}(\Phi, \Phi^*, T)$ zero at $T = 0$ in Eq. (8). The grand potential in the vacuum becomes the renormalization scale M dependent when the fermionic vacuum loop contribution in the first term of Eq. (17) gets replaced by the appropriately renormalized term of Eq. (24), and we write

$$\Omega^{\rm M}(\sigma_x, \sigma_y) = U(\sigma_x, \sigma_y) + \Omega^{\rm vac}_{q\bar{q}}. \tag{25}$$

The six unknown parameters—m^2, λ_1, λ_2, h_x, h_y, c—in the mesonic potential $\mathrm{U}(\sigma_x, \sigma_y)$ are determined from the σ_x- and σ_y-dependent expressions of meson masses, which are obtained by the double derivatives of the effective potential Eq. (25) with respect to different meson fields. The mathematical details for determining different parameters are given in Appendix A, where the logarithmic M dependence of the term $\Omega^{\rm vac}_{q\bar{q}}$ gives rise to a renormalization scale M-dependent part $\lambda_{2\mathrm{M}}$ in the expression of the parameter $\lambda_2 = \lambda_{2s} + n + \lambda_{2+} + \lambda_{2\mathrm{M}}$. λ_{2s} is the same old λ_2 parameter of the QM/PQM model in Refs. [29,35,44]. Here, $n = \frac{N_c g^4}{32\pi^2}$, $\lambda_{2+} = \frac{n f_\pi^2}{f_K(f_K - f_\pi)}\log\{\frac{2f_K - f_\pi}{f_\pi}\}$ and $\lambda_{2\mathrm{M}} = 4n\log\{\frac{g(2f_K - f_\pi)}{2\mathrm{M}}\}$. After substituting this value of λ_2 in the expression of $\mathrm{U}(\sigma_x, \sigma_y)$ and writing all the terms of summation in the $\Omega^{\rm vac}_{q\bar{q}}$ expression explicitly, Eq. (25) can be rewritten as

TABLE I. Parameters for $m_\sigma = 600$ MeV with and without $U_A(1)$ axial anomaly term.

Model	c [MeV]	m^2 [MeV^2]	λ_1	λ_{2s}	h_x [MeV^3]	h_y [MeV^3]
QM W/$U_A(1)$	4807.84	$(342.52)^2$	1.40	46.48	$(120.73)^3$	$(336.41)^3$
QMVT W/$U_A(1)$	4807.84	$-(184.86)^2$	−1.689	46.48	$(120.73)^3$	$(336.41)^3$
QM W/o$U_A(1)$	0	$-(189.85)^2$	−17.01	82.47	$(120.73)^3$	$(336.41)^3$
QMVT W/o$U_A(1)$	0	$-(424.68)^2$	−20.46	82.47	$(120.73)^3$	$(336.41)^3$

$$\Omega^{\mathrm{M}}(\sigma_x,\sigma_y)=\frac{m^2}{2}(\sigma_x^2+\sigma_y^2)-h_x\sigma_x-h_y\sigma_y-\frac{c}{2\sqrt{2}}\sigma_x^2\sigma_y+\frac{\lambda_1}{4}(\sigma_x^4+\sigma_y^4+2\sigma_x^2\sigma_y^2)+\frac{(\lambda_{2\mathrm{v}}+n+\lambda_{2\mathrm{M}})}{8}(\sigma_x^4+2\sigma_y^4)-\frac{n\sigma_x^4}{2}\log\left(\frac{g\sigma_x}{2\mathrm{M}}\right)-n\sigma_y^4\log\left(\frac{g\sigma_y}{\sqrt{2}\mathrm{M}}\right). \quad (26)$$

Here, $\lambda_{2\mathrm{v}}=\lambda_{2s}+\lambda_{2+}$. After rearrangement of terms, we find that the logarithmic M dependence of λ_2 contained in $\lambda_{2\mathrm{M}}$ completely cancels the scale dependence of all the terms in $\Omega_{q\bar{q}}^{\mathrm{vac}}$. The chiral part of the total effective potential now becomes free of any renormalization scale dependence. It is reexpressed as

$$\Omega(\sigma_x,\sigma_y)=\frac{m^2}{2}(\sigma_x^2+\sigma_y^2)-h_x\sigma_x-h_y\sigma_y-\frac{c}{2\sqrt{2}}\sigma_x^2\sigma_y+\frac{\lambda_1}{2}\sigma_x^2\sigma_y^2+\frac{\lambda_1}{4}(\sigma_x^4+\sigma_y^4)+\frac{(\lambda_{2\mathrm{v}}+n)}{8}(\sigma_x^4+2\sigma_y^4)-\frac{n\sigma_x^4}{2}\log\left(\frac{\sigma_x}{(2f_K-f_\pi)}\right)-n\sigma_y^4\log\left(\frac{\sqrt{2}\sigma_y}{(2f_K-f_\pi)}\right). \quad (27)$$

The calculation of vacuum meson masses from the effective potential also shows that the scale M dependence completely cancels out from their expressions. The explicit derivations of scale independent meson masses are given in Appendix B.

In general, m_π, m_K, the pion and kaon decay constant f_π, f_K, and mass squares of η, η', and m_σ are used to fix the six parameters of the model. The parameters are fitted such that, in vacuum, the model produces observed pion mass $m_\pi = 138$ MeV, kaon mass $m_K = 496$ MeV, and $m'_\eta = 963(138)$ MeV, $m_\eta = 539(634.8)$ MeV for the case with the presence (absence, $c = 0$) of axial anomaly term c. Numerical values of λ_{2s} and c are obtained easily after substituting the values of the input parameters in their expressions in Appendix A. Numerical values of λ_{2+} and n are obtained using $f_\pi = 92.4$, $f_K = 113$ MeV, and $N_c = 3$. The scale-independent expressions of m_π^2 and m_σ^2 given in Appendix B are exploited in Appendix A to obtain the vacuum values of the parameters m^2 and λ_1 using $m_\sigma = 600$ MeV. In the present work, the λ_{2s} and c are the same as in the QM model [35], the value of h_x and h_y are also not affected by the fermionic vacuum correction. The parameters that are modified by the fermionic vacuum correction are m^2, λ_1, and λ_2. Table I summarizes the numerical values of the parameters in different model scenarios. We point out that the effect of one-loop fermionic vacuum fluctuation in the 2 + 1 flavor renormalized PQM model has already been studied in the recent works of Refs. [84,85]. The model parameters (λ_2, λ_1, and m^2) in these investigations are renormalization scale dependent, and the cancellation of scale dependence for the final results is achieved numerically.

Now, the thermodynamic grand potential in the presence of appropriately renormalized fermionic vacuum contribution in the Polyakov quark meson model with vacuum term (PQMVT) model will be written as

$$\Omega_{\mathrm{MF}}(T,\mu;\sigma_x,\sigma_y,\Phi,\Phi^*)=\mathcal{U}(T;\Phi,\Phi^*)+\Omega(\sigma_x,\sigma_y)+\Omega_{q\bar{q}}^{\mathrm{T}}(T,\mu;\sigma_x,\sigma_y,\Phi,\Phi^*). \quad (28)$$

One can get the quark condensates σ_x, σ_y and Polyakov loop expectation values Φ, Φ^* by searching the global minima of the grand potential for a given value of temperature T and chemical potential μ,

$$\frac{\partial\Omega}{\partial\sigma_x}=\frac{\partial\Omega}{\partial\sigma_y}=\frac{\partial\Omega}{\partial\Phi}=\frac{\partial\Omega}{\partial\Phi^*}\Big|_{\sigma_x=\bar{\sigma}_x,\sigma_y=\bar{\sigma}_y,\Phi=\bar{\Phi},\Phi^*=\bar{\Phi}^*}=0. \quad (29)$$

IV. MESON MASSES AND MIXING ANGLES

The curvature of the grand potential in Eq. (12) at the global minimum gives the finite temperature scalar and pseudoscalar meson masses,

$$m_{\alpha,ab}^2\Big|_T=\frac{\partial^2\Omega_{\mathrm{MF}}(T,\mu;\sigma_x,\sigma_y,\Phi,\Phi^*)}{\partial\xi_{\alpha,a}\partial\xi_{\alpha,b}}\Big|_{\mathrm{min}}. \quad (30)$$

In the subscript α = s, p; "s" stands for scalar and "p" stands for pseudoscalar mesons and $a, b = 0\ldots8$,

$$m_{\alpha,ab}^2|_T=m_{\alpha,ab}^2+(\delta m_{\alpha,ab}^{\mathrm{T}})^2. \quad (31)$$

The temperature dependence of meson masses comes from the temperature dependence of σ_x and σ_y. The term $(\delta m_{\alpha,ab}^{\mathrm{T}})^2$ results from the explicit temperature dependence of quark-antiquark potential in the grand potential. It vanishes in the vacuum where the meson mass matrix is determined as

$$m^2_{\alpha,ab} = \frac{\partial^2 \Omega^{\mathrm{M}}(\sigma_x, \sigma_y)}{\partial \xi_{\alpha,a} \partial \xi_{\alpha,b}} \Bigg|_{\min} = (m^{\mathrm{m}}_{\alpha,ab})^2 + (\delta m^{\mathrm{v}}_{\alpha,ab})^2. \tag{32}$$

Here the expressions $(m^{\mathrm{m}}_{\alpha,ab})^2$ as originally evaluated in Refs. [29,35] represent the second derivatives of the pure mesonic potential $\mathrm{U}(\sigma_x, \sigma_y)$ at its minimum, and the vacuum values of meson masses, $m^2_{\alpha,ab}$, in the QM/PQM model are given only by these terms. The calculation details of mass modifications $(\delta m^{\mathrm{v}}_{\alpha,ab})^2$ resulting due to the fermionic vacuum correction are presented in Appendix A, where we have also shown how those expressions are used for determining the model parameters. Table IV of Appendix A contains all the expressions of $(m^{\mathrm{m}}_{\alpha,ab})^2$ and $(\delta m^{\mathrm{v}}_{\alpha,ab})^2$. The mass expressions $(m^{\mathrm{m}}_{\alpha,ab})^2$ have a renormalization scale M dependence in the QMVT/PQMVT model due to the parameter λ_2. This dependence gets completely canceled by the already existing scale M dependence in the mass modifications $(\delta m^{\mathrm{v}}_{\alpha,ab})^2$, and the final expressions of vacuum meson masses $m^2_{\alpha,ab}$ are free of any renormalization scale dependence as shown explicitly in Appendix B.

In order to further calculate the in-medium meson mass modifications at finite temperature due to the quark-antiquark contribution in the presence of the Polyakov loop potential, the complete dependences of all scalar and pseudoscalar meson fields in Eq. (6) have to be taken into account. We have to diagonalize the resulting quark mass matrix. In the following, we recapitulate the expressions of mass modification due to the quark-antiquark contribution at finite temperature in the PQM model [44] as

$$\begin{aligned}(\delta m^{\mathrm{T}}_{\alpha,ab})^2|_{\mathrm{PQM}} &= \frac{\partial^2 \Omega^{\mathrm{T}}_{q\bar{q}}(T, \mu, \sigma_x, \sigma_y, \Phi, \Phi^*)}{\partial \xi_{\alpha,a} \partial \xi_{\alpha,b}} \Bigg|_{\min} \\ &= 3 \sum_{f=x,y} \int \frac{d^3p}{(2\pi)^3} \frac{1}{E_f} \Bigg[(A^+_f + A^-_f) \\ &\quad \times \left(m^2_{f,ab} - \frac{m^2_{f,a} m^2_{f,b}}{2E^2_f} \right) + (B^+_f + B^-_f) \\ &\quad \times \left(\frac{m^2_{f,a} m^2_{f,b}}{2E_f T} \right) \Bigg]. \end{aligned} \tag{33}$$

Here $m^2_{f,a} \equiv \partial m^2_f / \partial \xi_{\alpha,a}$ denotes the first partial derivative and $m^2_{f,ab} \equiv \partial m^2_{f,a} / \partial \xi_{\alpha,b}$ signifies the second partial derivative of the squared quark mass with respect to the meson fields $\xi_{\alpha,b}$. These derivatives are evaluated in Table III of Ref. [35]. We have given this table in Appendix A. The notations $A^{\pm}_f$ and $B^{\pm}_f$ have the following definitions,

$$A^+_f = \frac{\Phi e^{-E^+_f/T} + 2\Phi^* e^{-2E^+_f/T} + e^{-3E^+_f/T}}{g^+_f} \tag{34}$$

$$A^-_f = \frac{\Phi^* e^{-E^-_f/T} + 2\Phi e^{-2E^-_f/T} + e^{-3E^-_f/T}}{g^-_f}, \tag{35}$$

and $B^{\pm}_f = 3(A^{\pm}_f)^2 - C^{\pm}_f$, where we again define

$$C^+_f = \frac{\Phi e^{-E^+_f/T} + 4\Phi^* e^{-2E^+_f/T} + 3e^{-3E^+_f/T}}{g^+_f} \tag{36}$$

$$C^-_f = \frac{\Phi^* e^{-E^-_f/T} + 4\Phi e^{-2E^-_f/T} + 3e^{-3E^-_f/T}}{g^-_f}. \tag{37}$$

In the PQMVT model, the final expression for finite temperature meson masses in Eq. (31) is written as

$$m^2_{\alpha,ab}|_{T,\mathrm{PQMVT}} = m^2_{\alpha,ab} + (\delta m^{\mathrm{T}}_{\alpha,ab})^2|_{\mathrm{PQM}}. \tag{38}$$

This expression gives meson masses in the PQM model also when the fermionic vacuum contribution becomes zero in the expression of vacuum meson masses in the first term. The expression for the finite temperature meson mass modifications $(\delta m^{\mathrm{T}}_{\alpha,ab})^2|_{\mathrm{QM}}$ due to the quark-antiquark potential in the QM model can be found in Ref. [35]. We use this expression to write the finite temperature meson masses in the QMVT model as

$$m^2_{\alpha,ab}|_{T,\mathrm{QMVT}} = m^2_{\alpha,ab} + (\delta m^{\mathrm{T}}_{\alpha,ab})^2|_{\mathrm{QM}}. \tag{39}$$

Here, also, the same expression gives meson masses in the QM model when the fermionic vacuum correction is absent in the expression of vacuum meson masses.

The diagonalization of (0–8) component of the mass matrix gives the masses of σ and f_0 mesons in the scalar sector and the masses of η' and η in the pseudoscalar sector. The scalar mixing angle θ_s and pseudoscalar mixing angle θ_p are given by

$$\tan 2\theta_\alpha = \left(\frac{2m^2_{\alpha,08}}{m^2_{\alpha,00} - m^2_{\alpha,88}} \right). \tag{40}$$

Appendix C of Ref. [35] contains all the transformation details of the mixing for the (0,8) basis that generates the physical basis of the scalar (σ, f_0) and pseudoscalar (η', η) mesons. This Appendix also explains the ideal mixing and gives the details of the formulas by which the physical mesons transform into the mesons which are pure strange or nonstrange quark systems.

V. FERMIONIC VACUUM CORRECTION AND CHIRAL RESTORATION

We are investigating the effect of fermionic vacuum fluctuation on the restoration of chiral symmetry when it is properly accounted for in the 2 + 1 flavor quark meson model and PQM model at finite temperature and zero chemical potential with and without axial $U_A(1)$ breaking. We have compared the results of present computations in the QMVT and PQMVT models with the already existing calculations in the quark meson model and PQM model [35,44]. The interplay of the effect of $U_A(1)$ axial restoration and chiral symmetry restoration in the influence of fermionic vacuum fluctuation has been investigated and

TABLE II. The table of characteristic temperature (pseudocritical temperature) for the chiral transition in the nonstrange sector T_c^{χ}, strange sector T_s^{χ}, and the confinement-deconfinement transition T_c^{Φ} in the QM, QMVT, PQM, and PQMVT models. $\pm$ gives the temperature range near T_s^{χ}, over which the rather flat and broad second peak of the strange condensate derivative $\frac{\partial \sigma_y}{\partial T}$ shows a distinct change of about 0.1% of the numerical value of the second peak height.

	QM	QMVT	PQM	PQMVT
T_c^{χ} (MeV)	146.1	171.1	205.8	216.5
T_s^{χ} (MeV)	248.3 $\pm$ 2.0	247.8 $\pm$ 2.5	274 $\pm$ 1.5	269. $\pm$ 4.0
T_c^{Φ} (MeV)	...	...	205.6	205.6

compared in different model scenarios through the temperature variation of strange, nonstrange chiral condensates, meson masses, and mixing angles. The $U_A(1)$ axial breaking term is constant throughout the computation. The value of Yukawa coupling $g = 6.5$ has been fixed from the nonstrange constituent quark mass $m_q = 300$ MeV in vacuum ($T = 0$, $\mu = 0$). This predicts the vacuum strange quark mass $m_s \backsimeq 433$ MeV.

A. Condensates and fermionic vacuum correction

The solutions of the gap equations (29) at zero chemical potential yield the temperature dependence of the Polyakov loop expectation value Φ; nonstrange and strange condensates and the inflection point of these order parameters, respectively, give the characteristic temperature (pseudocritical temperature) for the confinement-deconfinement transition T_c^{Φ} and the chiral transition in the nonstrange T_c^{χ} and strange sector T_s^{χ}. Table II shows the various pseudocritical temperatures in different models. We will use a reduced temperature scale T/T_c^{χ} to compare the PQMVT (QMVT) model variations with that of the PQM(QM) model because the absolute comparison of the characteristic temperatures between two models of the same universality class cannot be made according to the Ginsburg-Landau effective theory [73].

For $T = 0$, Fig. 1(a) shows that the condensate $\sigma_x = 92.4$ MeV, while $\sigma_y = 94.5$ MeV in Fig. 1(b). The $U_A(1)$ anomaly ($c \neq 0$) has a negligible effect on the nonstrange condensate σ_x variation, which is sharpest for the $T/T_c^{\chi} =$ 0.9–1.2 range in the PQM model. The σ_x variation becomes smoother in the PQMVT model on account of the fermionic vacuum correction, and its most smooth variation results in the QMVT model due to the absence of the Polyakov loop potential. The fermionic vacuum correction together with the Polyakov loop potential give rise to the largest degree of strange condensate σ_y melting in the PQMVT model when $c \neq 0$ in Fig. 1(b). The PQM model σ_y melting is already reported [44] to be significantly larger than that of the QM model. The effect of only the fermionic vacuum correction is quite robust as is evident from a noticeably larger melting of the σ_y in the QMVT model. Comparing the model results of the σ_y temperature variation for the $c = 0$ case with that of the $c \neq 0$ case in Fig. 1(b), we conclude that the melting of the strange condensate gets reduced in the same small proportion in all the models when the axial anomaly term is absent.

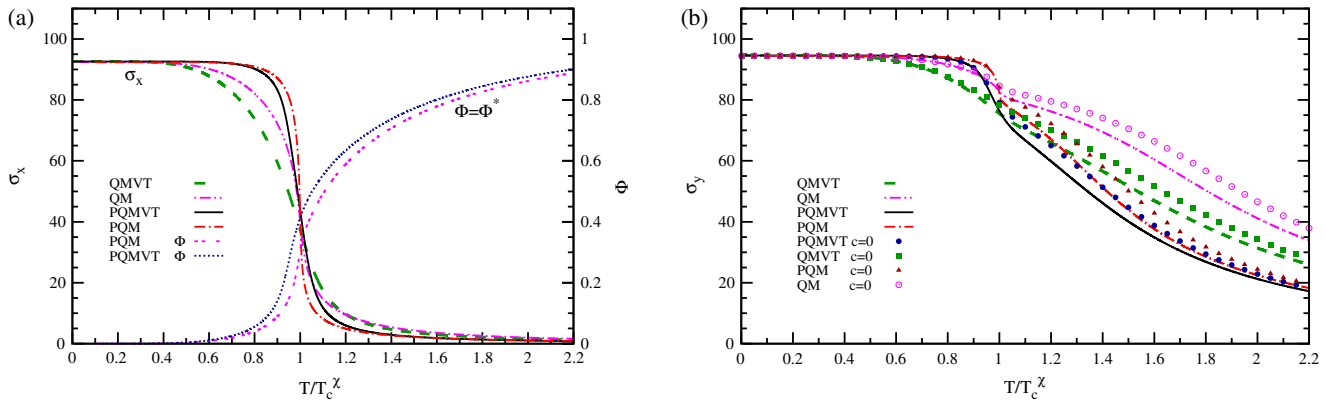

FIG. 1 (color online). Figure 1(a) shows the reduced temperature scale (T/T_c^{χ}) variation of the non strange condensate σ_x at zero chemical potential ($\mu = 0$) and the nonzero axial anomaly ($c \neq 0$) in the QM, QMVT, PQM, and PQMVT model calculations. The dash double dots line in magenta, the thick long dash line in dark green, and the dash dot line in red represent the respective σ_x variations in the QM, QMVT, and PQM models, while the solid black line represents the PQMVT model σ_x variation. The same line types in Fig. 1(b) represent the respective model variations of the strange condensate σ_y when $c \neq 0$. The line of solid circle dots in dark blue and the line of solid triangle dots in deep red in Fig. 1(b) show the respective variations of the σ_y in the PQMVT and PQM models, while the line of solid square dots in green and the line of hollow circle dots in magenta represent the respective σ_y variations in the QMVT and QM models when the axial anomaly term is absent, i.e., $c = 0$. The expectation value of the Polyakov loop field Φ is shown in the right side plots of Fig. 1(a) where the dotlike small dash line in dark blue represents the Φ variation in the PQMVT model, while the double dash line in magenta represents the Φ variation in the PQM model. (a) Nonstrange condensate variation with $U_A(1)$ anomaly term. (b) Strange condensate variation with and without $U_A(1)$ anomaly term.

Curves ending in the right side of Fig. 1(a) represent the temperature variation of the Polyakov loop expectation value Φ. Since $\mu = 0$ in our calculations, we have $\Phi = \Phi^*$. Here, we recall that the improved ansatz of the logarithmic Polyakov loop potential [10,54,55,63] avoids the Φ expectation value higher than one and hence describes the dynamics of gluons more effectively.

The peak in the temperature variation of $\frac{\partial \sigma_x}{\partial T}$ in Fig. 2(a) gives the T_c^{χ} for the chiral crossover at $\mu = 0$. It is evident from the plots in Fig. 2(a) and the values given in Table II that the fermionic vacuum correction causes a smoother and gentler crossover transition in the nonstrange sector, where the transition temperature T_c^{χ} for the PQMVT (QMVT) model increases by 10.7(25) MeV over its PQM (QM) model value. The confinement-deconfinement crossover transition temperature $T_c^{\Phi} = 205.6$ MeV is same in both the models, PQM and PQMVT. But unlike the PQM model, the deconfinement transition for the PQMVT model does not remain coincident with the nonstrange sector chiral crossover transition and we get $T_c^{\chi} > T_c^{\Phi}$. The chiral crossover is coincident with the confinement-deconfinement transition in the RBC-Bielefeld and HotQCD lattice calculations, where T_c^{χ} lies between 185–195 MeV [19–21], but the Wuppertal-Budapest(WB) Collaboration, in comparison, gives a pseudocritical temperature that is 40 MeV smaller for the nonstrange crossover transition and 15 MeV smaller for the deconfinement transition and $T_c^{\chi} < T_c^{\Phi}$ [22–24]. In our PQMVT model calculation, we have taken $m_\sigma = 600$ and $T_0 = 270$ MeV in order to compare results with the earlier work done in the QM and PQM models in Refs. [35,36,44]. This choice does not reproduce the Wuppertal-Budapest scenario and is more in tune with the standard scenario of the PQM model calculations of Schaefer *et al.* in Ref. [45], where they have done detailed comparisons of various transitions with different parameter sets and three different parametrizations of the Polyakov loop potential. The recent HotQCD lattice results show smaller disagreement in the transition temperature value [25] when compared with the WB results for the physical pion mass. We point out that most lattice calculations are carried out with periodic boundary condition, which is convenient for the computations, but rather far from the experimental setup. An exploratory quenched study [90] suggests that critical temperatures with realistic boundary conditions can be up to 30 MeV larger than the values, which are measured in conventional lattice calculations. In effective model investigations, the T_c^{χ} and T_c^{Φ} values are quite sensitive to the chosen models and parameter sets. In the NJL and PNJL model investigations [75], for example, the consideration of the eight quark interactions leads to the significant lowering of the pseudocritical temperature for the chiral crossover transition. Further, the smaller values of T_0 for the Polyakov loop potential also lead to considerable lowering of the transition temperature [53]. The parameters corresponding to $m_\sigma = 400$ MeV in our PQMVT model calculation give $T_c^{\chi} = 202.6$ MeV and $T_c^{\Phi} = 201.1$ MeV. Here, the nonstrange chiral crossover and deconfinement transitions are almost coincident similar to the recent results of Schaefer *et al.* [84] in the renormalized PQM model.

The chiral crossover transition in the strange sector is much smoother and weaker than the crossover transition of

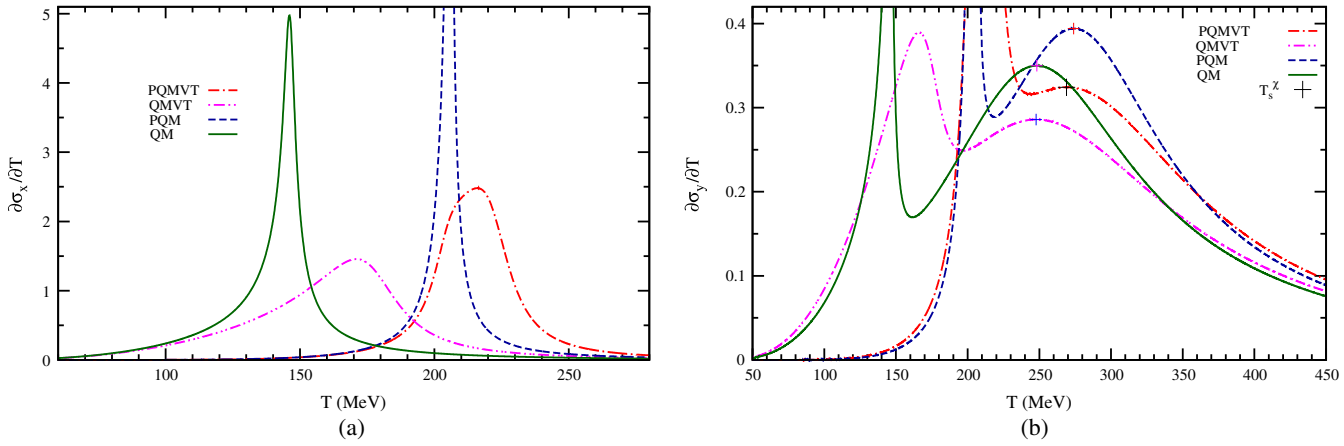

FIG. 2 (color online). (a) Shows the temperature variation of the $\frac{\partial \sigma_x}{\partial T}$. The dash dot in red, dash double dot in magenta, and solid line in dark green show the respective PQMVT, QMVT, and QM model variations with their distinct peaks. The dash line in dark blue shows the PQM model variation whose very high peak is not visible on the y-axis scale, which has been chosen to highlight the peaks for other model variations in Fig. 2(a). The same line types in Fig. 2(b) show the respective model temperature variations of the strange condensate temperature derivative $\frac{\partial \sigma_y}{\partial T}$. This variation shows two peaks where the first peak is caused by the chiral dynamics in the nonstrange sector. The location of the second peak [marked by the plus symbol in Fig. 2(b)] gives strange sector chiral crossover transition temperature T_s^{χ}. The second peak is very broad and flat over a small temperature range, and its location is marked by an ambiguity range of $\pm$ for the T_s^{χ} (given in Table II) in which the derivative $\frac{\partial \sigma_y}{\partial T}$ shows a distinct change of about 0.1% of the numerical value of the second peak height. (a) With $U_A(1)$ anomaly term. (b) With $U_A(1)$ anomaly term.

the nonstrange sector for all the models due to the large constituent mass of the strange quark $m_s = 433$ MeV in vacuum. The variation of the temperature derivative of σ_y shows two peaks in Fig. 2(b) for all the models; the first peak is higher and sharper because it is driven by the chiral crossover transition dynamics in the nonstrange sector. The crossover temperature T_s^{χ} in the strange sector is identified in Fig. 2(b) by locating the position of the second peak which is quite broad, smooth, and flat over a small temperature range in all the models. The ambiguity in the identification of the second peak [marked by the plus symbol in Fig. 2(b)] is indicated by the $\pm$ flatness range for T_s^{χ} in Table II. The largest but smoother melting of the strange condensate is obtained in the PQMVT model with $T_s^{\chi} = 269.0 \pm 4$ MeV. It will have an interesting physical consequence in the early setting up of a smoother mass degeneration trend in masses of the chiral partners (K, κ) and (η, f_0) and in the early emergence of a smoother $U_A(1)$ restoration trend.

B. Meson mass variations

The meson mass temperature variations of the PQMVT (QMVT) model in the presence of the axial $U_A(1)$ anomaly term are compared with the corresponding PQM(QM) model results, respectively, in Fig. 3(a) [Fig. 3(b)] for the chiral partners (σ, π) and (a_0, η') and in Fig. 5(a) [Fig. 5(b)] for the chiral partners (η, f_0) and (K, κ). The analogous plots of mass variations when the axial $U_A(1)$ anomaly term $(c = 0)$ is absent are given, respectively, in Fig. 4(a) [Fig. 4(b)] and Fig. 6(a) [Fig. 6(b)].

The sharpest mass degeneration of the PQM model for the (σ, π) and (a_0, η') mesons becomes quite smooth in Fig. 3(a) for the PQMVT model due to the smoother melting of the nonstrange condensate σ_x caused by the fermionic vacuum correction in Fig. 1(a). The most smooth mass degeneration results are in Fig. 3(b) for the QMVT model variations because the Polyakov loop effect which causes a sharper chiral crossover transition is absent. A similar trend of smoother mass degeneration is seen in the masses of the chiral partners (η, f_0) and (K, κ) in Fig. 5(a) [Fig. 5(b)] for the PQMVT(QMVT) model. Since a significant melting of the strange condensate σ_y occurs at a higher temperature in all the models, the K, κ, and η meson masses become degenerate not exactly at $T/T_c^{\chi} = 1$ but around $T/T_c^{\chi} = 1.3(1.2)$ in the PQMVT(PQM) model. The f_0 meson mass intersects the degenerate line of K, κ, and η meson masses around $T/T_c^{\chi} = 1.4(1.8)$ in Fig. 5(a) [Fig. 5(b)] for the PQM(QM) model computations and then becomes smaller than the m_{η}, developing a kinklike structure after crossing it. Later, the f_0 meson mass degenerates with the m_K, m_{κ}, and m_{η} variations again for $T/T_c^{\chi} > 1.8(2.3)$. We find that the kink in the f_0 meson mass variation altogether disappears from the PQMVT(QMVT) model results in Fig. 5(a) [Fig. 5(b)] due to the robust effect of the fermionic vacuum correction, and the m_{f_0} degenerates quite smoothly with the m_K, m_{κ}, and m_{η} earlier at $T/T_c^{\chi} > 1.7(1.9)$ and remains so forever. These mass degeneration trends reflect the effect of fermionic vacuum fluctuation on the chiral symmetry restoration in the strange sector and result due to the smoother but larger (largest in the PQMVT model) melting of the strange condensate in Fig. 1(b).

The PQM (QM) model σ meson mass variation also shows a kink structure that starts at $T/T_c^{\chi} = 1.5(1.9)$ and persists afterwards in Fig. 3(a) [Fig. 3(b)]. This kink again disappears from the m_{σ} variations in the PQMVT and QMVT model, where the smooth line of the degenerated

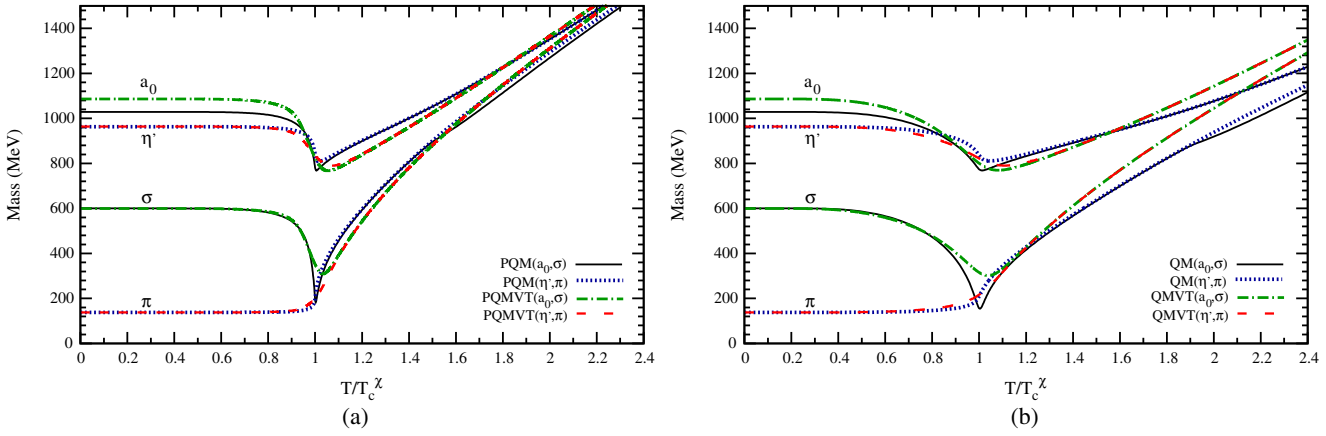

FIG. 3 (color online). Mass variations for the chiral partners (σ, π) and (a_0, η') on the reduced temperature (T/T_c^{χ}) scale at $\mu = 0$ are plotted in Fig. 3(a) for the PQMVT and PQM model, and the corresponding mass variations in the QMVT and QM model are plotted in Fig. 3(b). The dash dot line plots in dark green and the solid line plots in black, respectively, for the PQMVT(QMVT) model and the PQM(QM) model show the σ and a_0 mass variations in the left panel (right panel). The π and η' mass variations are denoted by the dash line in red plots and the thick dots line in blue plots, respectively, for the PQMVT(QMVT) model and the PQM(QM) model in the left panel(right panel). (a) PQMVT and PQM model results:axial anomaly term $c \neq 0$. (b) QMVT and QM model results: axial anomaly term $c \neq 0$.

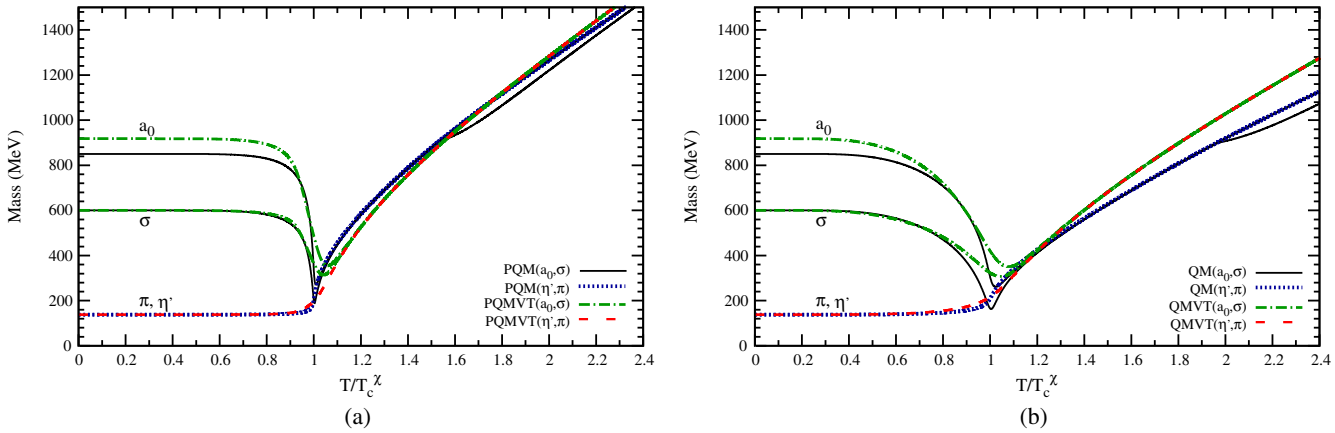

FIG. 4 (color online). The line types in Figs. 4(a) and 4(b) represent the same mass variations as depicted in Fig. 3, but here in these computations the axial $U_A(1)$ anomaly term is absent, i.e., $c = 0$. (a) PQMVT and PQM model results:axial anomaly term $c = 0$. (b) QMVT and QM model results:axial anomaly term $c = 0$.

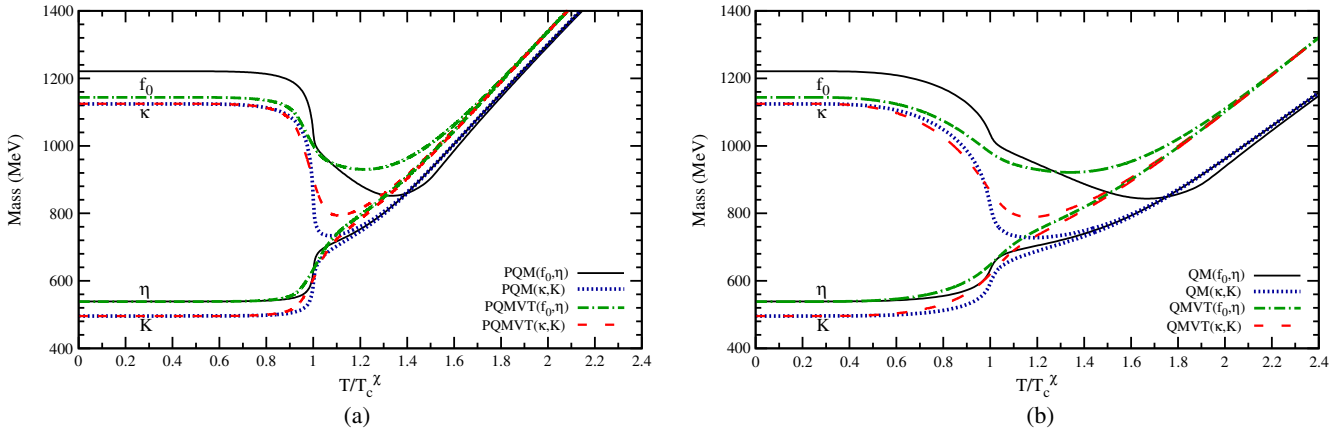

FIG. 5 (color online). Mass variations for the chiral partners (η, f_0) and (K, κ) on the reduced temperature (T/T_c^χ) scale at $\mu = 0$ are plotted in Fig. 5(a) for the PQMVT and PQM model and the corresponding mass variations in the QMVT and QM model, are plotted in Fig. 5(b). The dash dot line plots in dark green and the solid line plots in black, respectively, for the PQMVT(QMVT) model and the PQM(QM) model show the η and f_0 mass variations in the left panel(right panel). The K and κ mass variations are denoted by the dash line red plots and the thick dots line in blue plots, respectively, for the PQMVT(QMVT) model and the PQM(QM) model in the left panel(right panel). (a) PQMVT and PQM model results:axial anomaly term $c \neq 0$. (b) QMVT and QM model results:axial anomaly term $c \neq 0$.

m_σ and m_π in Figs. 3(a) and 3(b) show closer convergence towards the degenerate masses of a_0 and η' mesons for higher $T/T_c^\chi > 1$, and the mass gap between these two sets of chiral partners becomes small in comparison to the mass gap seen in the PQM and QM models. Here, we recall that the $U_A(1)$ axial symmetry breaking generates the mass gap between the two sets of the chiral partners, (σ, π) and (a_0, η'), i.e., $m_\pi = m_\sigma < m_{a_0} = m_{\eta'}$ for $T/T_C^\chi > 1$ because the anomaly term $(\frac{c\sigma_y}{\sqrt{2}})$ has the opposite sign in the expressions of m_{a_0} and m_π [35]. Hence, the mass gap reduction will be larger due to the larger melting of σ_y for higher T/T_c^χ in the PQMVT model. We thus conclude that apart from affecting the smoother occurrence of chiral $SU_L(2) \times SU_R(2)$ symmetry restoration in the nonstrange sector, the inclusion of fermionic vacuum fluctuation in the PQM (QM) model also affects an early and smoother set up of the $U_A(1)$ restoration trend.

In the absence of the axial anomaly $c = 0$, the $m_{\eta'}$ always remains equal to m_π, and the mass degeneration of the chiral partners (σ, π) and (a_0, η') results near $T/T_c^\chi = 1.0$ in all the model plots. Here, also, the PQM (QM) model prominent kink structure, which forms near $T/T_c^\chi = 1.5(1.9)$ in the m_σ variation in Fig. 4(a) [Fig. 4(b)], gets completely smoothed out in the PQMVT(QMVT) model. Further, in Fig. 6(a) [Fig. 6(b)], the m_{f_0} variation in the PQM (QM) model for the $c = 0$ case does not become completely degenerate with the m_η, though it becomes very close to (nearly touches) the η mass variation when $T/T_c^\chi \sim 1.6(2.0)$, and afterwards m_{f_0} takes slightly larger value than the m_η. The f_0 mass variation, in contrast, degenerates

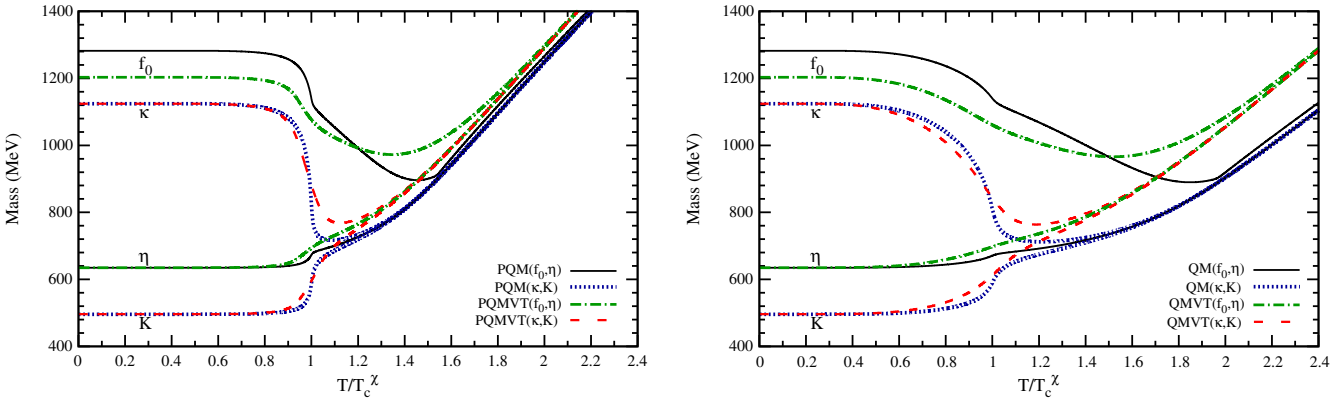

FIG. 6 (color online). The line types in Figs. 6(a) and 6(b) represent the same mass variations as depicted in Fig. 5, but here in these computations the axial $U_A(1)$ anomaly term is absent, i.e., $c = 0$. (a) PQMVT and PQM model results:axial anomaly term $c = 0$. (b) QMVT and QM model results:axial anomaly term $c = 0$.

quite smoothly with the m_η when $T/T_c^\chi \sim 1.9(2.3)$ in the PQMVT (QMVT) model. Thus, the fermionic vacuum correction leads to the smoother mass degeneration trends also when $c = 0$.

Here we mention another noteworthy result. In the influence of the fermionic vacuum correction, the scalar particle vacuum mass increases to 1086.26(917.93) MeV for the a_0 meson and decreases to 1143.92(1203.16) MeV for the f_0 meson in the presence(absence) of the axial anomaly in the QMVT/PQMVT model from the respective vacuum mass value of $m_{a_0} = 1028.7(850.5)$ MeV and $m_{f_0} = 1221.1(1282.3)$ MeV in the QM/PQM model. Further, we point out that the kinks in the PQM/QM model m_σ and m_{f_0} variations are the consequence of an interchange in their identities for higher values on the reduced temperature scale [35,44]. Here, we again emphasize that the crossing or anticrossing pattern in the meson mass variations completely disappears when the fermionic vacuum fluctuation is accounted for in the PQMVT and QMVT models. In order to have a proper perspective of the PQM/QM model kink structures and the complete washing out of such kinks in the PQMVT/QMVT model results, one has to investigate, analyze, and compare the scalar and pseudoscalar meson mixing angles.

C. Meson mixing angle variations

We will finally be investigating the behavior of the scalar θ_S and pseudoscalar θ_P mixing angles. In Fig. 7(a), the lower (upper) solid line in black and the dash dot line in red depict the θ_P (θ_S) variations, respectively, in the PQMVT and PQM model computations for nonzero axial anomaly. In the absence of axial anomaly, the dotlike small dash line in magenta and the dash line in dark blue represent the respective scalar mixing angle θ_S variations for the PQMVT and PQM models. The same line types in Fig. 7(b) show the θ_P and θ_S variations for the QMVT and the QM models. The pseudoscalar θ_P mixing angle variations shown by the filled green circles in both the figures are constant when the axial anomaly is zero in all the model calculations. Comparing the PQMVT(QMVT) model variations of θ_P and θ_S in Fig. 7(a) [Fig. 7(b)] with the corresponding PQM(QM) model results, we infer that the fermionic vacuum correction significantly modifies the axial $U_A(1)$ restoration pattern.

The nonstrange and strange quark mixing is strong as in Ref. [35], and one gets almost constant pseudoscalar mixing angle $\theta_P = -5°$ in all the models when the axial anomaly is present for the chiral symmetry broken phase at $T = 0$. The θ_P variation near $T/T_c^\chi = 1$ in the PQMVT model in Fig. 7(a) develops a small dip and then smoothly starts the approach toward the ideal mixing angle $\theta_P \rightarrow \arctan\frac{1}{\sqrt{2}} \sim 35°$; the corresponding $\Phi_P = 90°$. Here Φ_P is the pseudoscalar mixing angle in the strange-nonstrange basis (see Ref. [35] for details). In computations with the presence of the axial anomaly for $T/T_c^\chi > 1$, the pseudoscalar mixing angle approaches its ideal value more smoothly in the PQMVT(QMVT) model when compared with the corresponding result in the PQM(QM) model in Fig. 7(a) [Fig. 7(b)]. This approach is sharpest in the PQM model.

The η and η' mesons become a purely strange η_S and nonstrange η_{NS} quark system as a consequence of the ideal pseudoscalar mixing that gets fully achieved at higher values of the reduced temperature. In order to show this and make comparisons, the mass variations for the physical η, η' and the nonstrange-strange η_{NS}, η_S complex are plotted for the PQMVT(QMVT) and PQM(QM) models in Fig. 8(a) [Fig. 8(b)]. Mass formula $m_{\eta_{NS}}$ and m_{η_S} are given in Table V of Appendix B. In the $m_{\eta'}$ approach to $m_{\eta_{NS}}$ and the m_η approach to m_{η_S} around $T/T_c^\chi = 1$, the most smooth and smoother mass convergence trends are seen, respectively, in the QMVT and PQMVT models in Fig. 8(b) and Fig. 8(a). Comparing the mass difference of $m_{\eta'}$ and m_η for $T/T_c^\chi > 1$ in different models, the smallest difference seen in the PQMVT model indicates that, here,

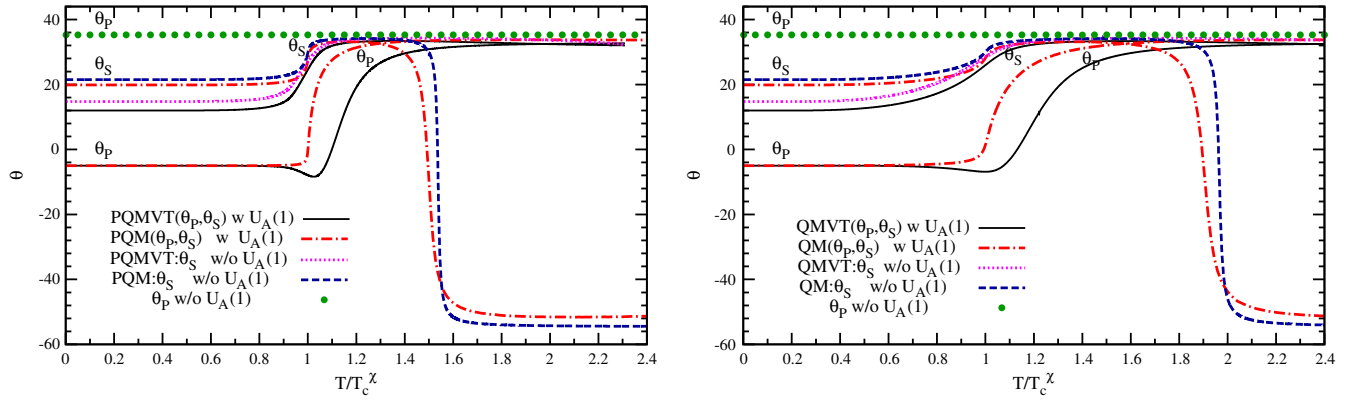

FIG. 7 (color online). In the presence of the axial anomaly, the lower(upper) black solid line and dash dot line in red depict the θ_P (θ_S) variations, respectively, in the PQMVT and PQM model computations in Fig. 7(a), while the same line types represent the corresponding variations, respectively, for the QMVT and QM models in Fig. 7(b). In the absence of the axial anomaly, i.e., $c = 0$, the dotlike small dash line in magenta and dash line in dark blue represent the scalar θ_S mixing angle variations, respectively, in the PQMVT and PQM model computations in Fig. 7(a), while the same line types represent the corresponding variations, respectively, for the QMVT and QM models in Fig. 7(b). The pseudo-θ_P mixing angle variations for $c = 0$ are constant and are shown by the dark green filled circular dots for both the PQMVT and PQM model calculations in Fig. 7(a), while the same line type represents the θ_P variations for the QMVT and QM model in Fig. 7(b). (a) Scalar and Pseudo scalar mixing angle variations in PQMVT and PQM model. (b) Scalar and Pseudo scalar mixing angle variations in QMVT and QM model.

we are getting the most converging $U_A(1)$ restoration trend on account of the fermionic vacuum term.

The fermionic vacuum correction gives rise to a decreased scalar mixing angle θ_S in vacuum ($T = 0$). It becomes 11.98°(14.75°) in the presence(absence) of the axial anomaly in the PQMVT and QMVT models in Figs. 7(a) and 7(b), respectively, from its value of 19.86°(21.5°) in the PQM and QM models. The θ_S growth to its ideal value near $T/T_c^\chi = 1$ is smoother in the PQMVT and QMVT models. The most striking effect of the fermionic vacuum correction can be seen in the complete modification of the θ_S behavior in the higher-temperature chirally symmetric phase of the PQMVT and QMVT models for both the cases with and without the axial anomaly. Instead of dropping down to the negative values as in the chiral symmetry restored phase of the PQM and QM models, respectively, in Figs. 7(a) and 7(b), the θ_S in the PQMVT and QMVT models approaches the ideal mixing angle very smoothly analogous to the pseudoscalar mixing angle θ_P temperature variation computed in the presence of axial anomaly.

In the chirally symmetric phase of the PQM and QM models, respectively, in Figs. 7(a) and 7(b), the scalar mixing angle first achieves its ideal value of 35° and

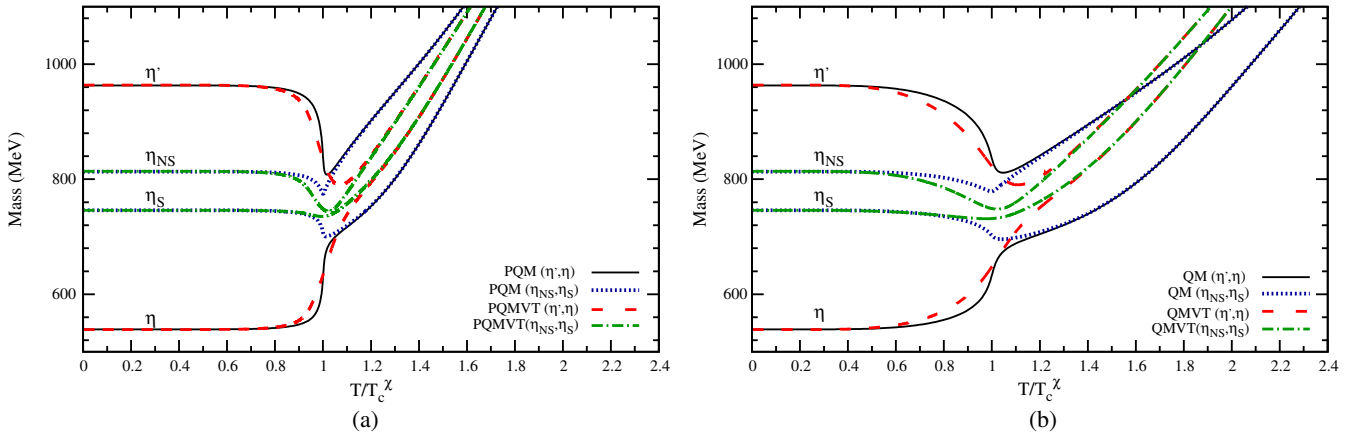

FIG. 8 (color online). Shows the mass variations for the physical η', η and the nonstrange-strange η_{NS}, η_S complex on the reduced temperature scale (T/T_c^χ) at zero chemical potential ($\mu = 0$). Figure 8(a) shows the results for PQMVT and PQM models and line types for mass variations are labeled. Figure 8(b) shows the mass variations for the QMVT and QM models with labeled line types. (a) With $U_A(1)$ anomaly term. (b) With $U_A(1)$ anomaly term.

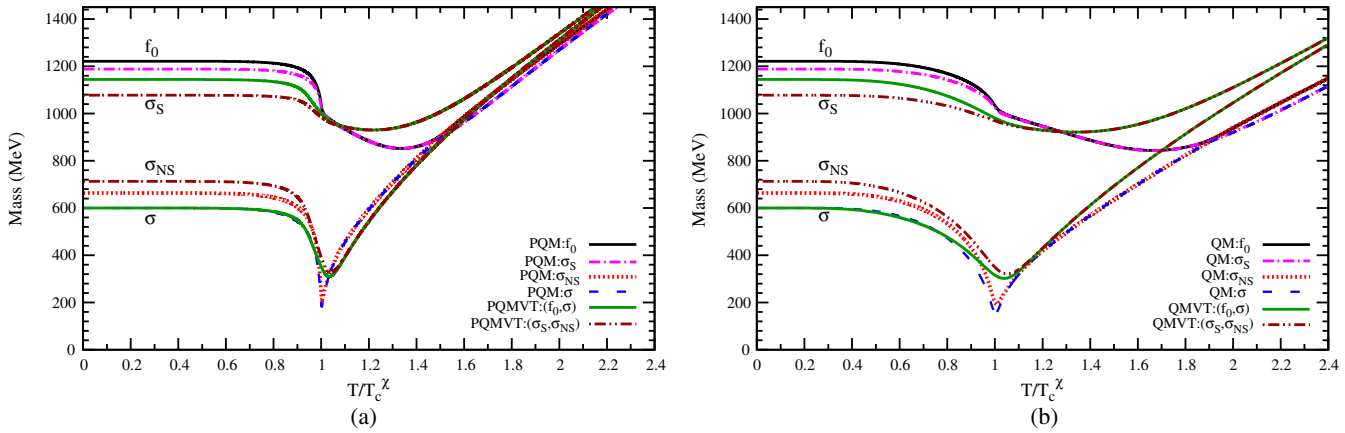

FIG. 9 (color online). Shows the mass variations for the physical σ, f_0 and the nonstrange-strange σ_{NS}, σ_S complex, on the reduced temperature scale (T/T_c^{χ}) at zero chemical potential ($\mu = 0$). Figure 9(a) shows the results for the PQMVT and PQM models and line types for mass variations are labeled. Figure 9(b) shows the mass variations for the QMVT and QM models with labeled line types. The masses of the physical σ and f_0 anticross and the nonstrange-strange $\sigma_{NS} - \sigma_S$ system masses cross for the PQM/QM model variations. Such crossing and anticrossing of masses disappears from the PQMVT/QMVT model results. (a) With $U_A(1)$ anomaly term. (b) With $U_A(1)$ anomaly term.

then drops down to $\theta_S \sim -51°(-54°)$ for higher temperatures in the presence (absence) of $U_A(1)$ axial symmetry breaking term. This drop happens around $T/T_c^{\chi} \sim 1.5(1.9)$ in the PQM(QM) model for nonzero c, and a similar drop for the calculations without the axial anomaly occurs at a little higher value of T/T_c^{χ}. This pattern is already reported and discussed in Refs. [35,44]. We note that when $\theta_S \sim 35°$, the f_0 meson degenerates with the pure strange quark system σ_S, while the σ meson becomes identical with the pure nonstrange quark system σ_{NS}. Since the mixing angle $\sim -55°$ is complimentary to 35°, (their difference is ~90°), the temperature variations of masses show a mass reversal trend in the nonstrange-strange basis when $\theta_S \sim -51°$, and the physical σ and f_0 masses anticross while the nonstrange-strange ($\sigma_{NS} - \sigma_S$) system masses cross near the above- mentioned reduced temperatures. After anticrossing, the physical σ becomes identical with the pure strange quark system σ_S, while the physical f_0 degenerates with the pure nonstrange quark system σ_{NS}. In order to show this crossing-anticrossing behavior in the presence of the axial anomaly, we have plotted in Figs. 9(a) and 9(b) the respective PQM and QM model mass variations for the physical σ and f_0 and the nonstrange-strange σ_{NS}, σ_S complex. Since the effect of fermionic vacuum fluctuation drastically modifies the θ_S behavior for higher temperatures, the masses of the physical σ and f_0 do not anticross, the nonstrange-strange ($\sigma_{NS} - \sigma_S$) system masses do not cross for higher values on the reduced temperature scale, and the σ becomes identical with the pure nonstrange quark system σ_{NS}, while the physical f_0 smoothly degenerates with the pure strange quark system σ_S in the PQMVT and QMVT model plots, respectively, in Figs. 9(a) and 9(b). Here, the θ_S approaches ~35° and then remains the same for higher temperatures.

VI. SUMMARY AND CONCLUSION

In the present paper, we have investigated how the inclusion of properly renormalized fermionic vacuum fluctuation in the 2 + 1 flavor QM and PQM models modifies the finite temperature behavior of masses and mixing angles of scalar and pseudoscalar mesons. It has been explicitly shown that expressions for the model parameters, meson masses, and mixing angles do not depend on any arbitrary renormalization scale. We explored the qualitative and quantitative effects of fermionic vacuum correction on the emerging mass degeneration patterns in the temperature variations of masses of the chiral partners in pseudoscalar (π, η, η', K) and scalar (σ, a_0, f_0, κ) meson nonets. From the mass convergence patterns, we identified chiral symmetry and $U_A(1)$ restoration trends and compared them in different model scenarios.

The fermionic vacuum correction causes a smoother and gentler crossover transition in the nonstrange sector, where the transition temperature T_c^{χ} for the PQMVT(QMVT) model increases by 10.7(25) MeV over its PQM(QM) model value. Unlike the PQM model result, the deconfinement crossover transition is not coincident with the nonstrange sector chiral crossover transition for the PQMVT model calculation with $m_{\sigma} = 600$, $T_0 = 270$ MeV and the logarithmic ansatz for the Polyakov loop potential. However, for $m_{\sigma} = 400$ MeV in the PQMVT model, we get $T_c^{\chi} = 202.6$ MeV and $T_c^{\Phi} = 201.1$ MeV. The sharpest PQM model σ_x variation for the $T/T_c^{\chi} = 0.9$ to 1.2 range becomes smoother and gentler in the PQMVT model. The QM model σ_x temperature variation becomes much smoother in the QMVT model only due to the effect of the fermionic vacuum correction term. The significant σ_y melting of the PQM model gets further enhanced on account of the fermionic vacuum correction, and we obtain

the largest but smoother melting of the strange condensate in the PQMVT model.

The sharpest mass degeneration of the PQM model for the (σ, π) and (a_0, η') mesons becomes quite smooth in the PQMVT model and the most smooth mass degeneration results in the QMVT model. We conclude from the behavior of these chiral partners that the chiral $SU_L(2) \times SU_R(2)$ symmetry restoring transition in the nonstrange sector becomes quite smooth on account of the fermionic vacuum correction. In its influence, the chiral symmetry restoration in the strange sector also becomes quite smooth, and similar trends of smoother mass degeneration can be seen in the PQMVT/QMVT model temperature variations of the masses of the chiral partners (η, f_0) and (K, κ). It is worth emphasizing that the kink structure in the PQM/QM model m_σ and m_{f_0} temperature variations altogether disappears from the corresponding PQMVT/QMVT model results due to the noteworthy effect of the fermionic vacuum correction, and the m_{f_0} degenerates quite smoothly with the m_K, m_κ, and m_η. Further, the smoothly merged line of m_σ and m_π shows a closer and narrower convergence to the degenerate line of m_{a_0} and m'_η for higher $T/T_c^\chi > 1$ in the PQMVT/QMVT models. This behavior is a consequence of the largest but smoother melting of the σ_y in the PQMVT model because the $U_A(1)$-breaking anomaly effect that leads to the mass gap between the two sets of the chiral partners, (σ, π) and (a_0, η'), i.e., $m_\pi = m_\sigma < m_{a_0} = m_{\eta'}$ for $T/T_C^\chi > 1$, is proportional to the strange condensate σ_y. Thus, the incorporation of the fermionic vacuum correction in the PQM/QM model also affects an early setup of the $U_A(1)$ restoration trend on the reduced temperature scale.

The pseudoscalar mixing angle θ_P in its approach to the ideal limit for $T/T_c^\chi > 1$ also looks quite smoother in the PQMVT/QMVT model calculations with the axial anomaly. The smallest mass difference between the $m_{\eta'}(= m_{\eta_{NS}})$ and $m_\eta(= m_{\eta_S})$ for $T/T_c^\chi > 1$, results in the PQMVT model. It shows that the fermionic vacuum correction generates a most effective $U_A(1)$ restoration trend in the pseudo scalar sector. Further in its influence, the scalar mixing angle θ_S in the vacuum $(T = 0)$ decreases to $11.98°(14.75°)$ in the presence(absence) of the axial anomaly in the PQMVT/QMVT models from its value of $19.86°(21.5°)$ for the PQM/QM models. In the chirally restored phase of the PQMVT/QMVT models, the fermionic vacuum correction drastically modifies the PQM model behavior for scalar mixing angle which instead of becoming negative, approaches its ideal value $\theta_S \sim 35°$ quite smoothly for higher temperatures in both the presence and absence of the axial anomaly. As a consequence, unlike the PQM model, masses of the physical σ and f_0 do not anticross, and the nonstrange-strange $(\sigma_{NS} - \sigma_S)$ system masses do not cross. The σ becomes identical with the pure nonstrange quark system σ_{NS}, while the physical f_0 smoothly degenerates with the pure strange quark system σ_S, and their mass variations become free of kink structure.

ACKNOWLEDGMENTS

Valuable suggestions and computational help given by Rajarshi Ray during the completion of this work are specially acknowledged. I am very much thankful to Rajarshi Tiwari for helping me generate quality colored figures. General physics discussions with Ajit Mohan Srivastava were very helpful. Computational support of the computing facility developed by the Nuclear Particle Physics group of the Physics Department, Allahabad University, under the Center of Advanced Studies(CAS) funding of UGC, India, is also acknowledged.

APPENDIX A: RENORMALIZED MODEL PARAMETERS

The mass modification in vacuum $(T = 0, \mu = 0)$ due to the fermionic vacuum correction will be given by

$$(\delta m^{\rm v}_{\alpha,ab})^2 = \frac{\partial^2 \Omega^{\rm vac}_{q\bar{q}}}{\partial \xi_{\alpha,a} \partial \xi_{\alpha,b}}\bigg|_{\rm min} = -\frac{N_c}{8\pi^2}\sum_f \bigg[\bigg(2\log\bigg(\frac{m_f}{\rm M}\bigg)+\frac{3}{2}\bigg)\bigg(\frac{\partial m_f^2}{\partial \xi_{\alpha,a}}\bigg)\bigg(\frac{\partial m_f^2}{\partial \xi_{\alpha,b}}\bigg) + \bigg(\frac{m_f^2}{2}+2m_f^2\log\bigg(\frac{m_f}{\rm M}\bigg)\bigg)\frac{\partial^2 m_f^2}{\partial \xi_{\alpha,a}\partial \xi_{\alpha,b}}\bigg]. \quad \text{(A1)}$$

Here, $|_{\rm min}$ stands for the global minimum of the full grand potential in Eq. (12). The first $m^2_{f,a} \equiv \partial m_f^2/\partial \xi_{\alpha,a}$ and second $m^2_{f,ab} \equiv \partial m^2_{f,a}/\partial \xi_{\alpha,b}$ partial derivatives of squared quark mass with respect to the meson fields as evaluated in Ref. [35] in the nonstrange-strange basis are presented in Table III. We have evaluated the mass modifications given in Eq. (A1) and collected different expressions of $(\delta m^{\rm v}_{\alpha,ab})^2$

TABLE III. First and second derivative of squared quark mass in nonstrange-strange basis with respect to meson fields are evaluated at minimum. The symbol x in the first two columns denotes the sum over two light flavors. The last two columns have only strange quark mass flavor denoted by symbol y.

		$m^2_{x,a}m^2_{x,b}/g^4$	$m^2_{x,ab}/g^2$	$m^2_{y,a}m^2_{y,b}/g^4$	$m^2_{y,ab}/g^2$
σ_0	σ_0	$\frac{1}{3}\sigma_x^2$	$\frac{2}{3}$	$\frac{1}{3}\sigma_y^2$	$\frac{1}{3}$
σ_1	σ_1	$\frac{1}{2}\sigma_x^2$	1	0	0
σ_4	σ_4	0	$\sigma_x\frac{\sigma_x+\sqrt{2}\sigma_y}{\sigma_x^2-2\sigma_y^2}$	0	$\sigma_y\frac{\sqrt{2}\sigma_x+2\sigma_y}{2\sigma_y^2-\sigma_x^2}$
σ_8	σ_8	$\frac{1}{6}\sigma_x^2$	$\frac{1}{3}$	$\frac{2}{3}\sigma_y^2$	$\frac{2}{3}$
σ_0	σ_8	$\frac{\sqrt{2}}{6}\sigma_x^2$	$\frac{\sqrt{2}}{3}$	$-\frac{\sqrt{2}}{3}\sigma_y^2$	$-\frac{\sqrt{2}}{3}$
π_0	π_0	0	$\frac{2}{3}$	0	$\frac{1}{3}$
π_1	π_1	0	1	0	0
π_4	π_4	0	$\sigma_x\frac{\sigma_x-\sqrt{2}\sigma_y}{\sigma_x^2-2\sigma_y^2}$	0	$\sigma_y\frac{\sqrt{2}\sigma_x-2\sigma_y}{\sigma_x^2-2\sigma_y^2}$
π_8	π_8	0	$\frac{1}{3}$	0	$\frac{2}{3}$
π_0	π_8	0	$\frac{\sqrt{2}}{3}$	0	$-\frac{\sqrt{2}}{3}$

TABLE IV. Expressions for $(m^{\mathrm{m}}_{\alpha,ab})^2$ in the left half of the table are the vacuum meson masses calculated from the second derivatives of the pure mesonic potential $\mathrm{U}(\sigma_x, \sigma_y)$. Evaluated expressions of mass modifications $(\delta m^{\mathrm{v}}_{\alpha,ab})^2$ due to the fermionic vacuum correction are given in the right half. Symbols used in the expressions are defined as $x = \sigma_x$, $y = \sigma_y$, $X = (1 + 4\log(\frac{g\sigma_x}{2\mathrm{M}}))$, and $Y = (1 + 4\log(\frac{g\sigma_y}{\sqrt{2}\mathrm{M}}))$.

	Meson masses calculated from pure mesonic potential		Fermionic vacuum correction in meson masses
$(m^{\mathrm{m}}_{a_0})^2$	$m^2 + \lambda_1(x^2+y^2) + \frac{3\lambda_2}{2}x^2 + \frac{\sqrt{2}c}{2}y$	$(\delta m^{\mathrm{v}}_{s,11})^2$	$-\frac{N_c g^4}{64\pi^2}x^2(4+3X)$
$(m^{\mathrm{m}}_{\kappa})^2$	$m^2 + \lambda_1(x^2+y^2) + \frac{\lambda_2}{2}(x^2+\sqrt{2}xy+2y^2) + \frac{c}{2}x$	$(\delta m^{\mathrm{v}}_{s,44})^2$	$-\frac{N_c g^4}{64\pi^2}(\frac{x+\sqrt{2}y}{x^2-2y^2})(x^3X - 2\sqrt{2}y^3Y)$
$(m^{\mathrm{m}}_{s,00})^2$	$m^2 + \frac{\lambda_1}{3}(7x^2+4\sqrt{2}xy+5y^2) + \lambda_2(x^2+y^2) - \frac{\sqrt{2}c}{3}(\sqrt{2}x+y)$	$(\delta m^{\mathrm{v}}_{s,00})^2$	$-\frac{N_c g^4}{96\pi^2}(3(x^2X+y^2Y)+4(x^2+y^2))$
$(m^{\mathrm{m}}_{s,88})^2$	$m^2 + \frac{\lambda_1}{3}(5x^2-4\sqrt{2}xy+7y^2) + \lambda_2(\frac{x^2}{2}+2y^2) + \frac{\sqrt{2}c}{3}(\sqrt{2}x-\frac{y}{2})$	$(\delta m^{\mathrm{v}}_{s,88})^2$	$-\frac{N_c g^4}{96\pi^2}(\frac{3}{2}(x^2X+4y^2Y)+2(x^2+4y^2))$
$(m^{\mathrm{m}}_{s,08})^2$	$\frac{2\lambda_1}{3}(\sqrt{2}x^2-xy-\sqrt{2}y^2) + \sqrt{2}\lambda_2(\frac{x^2}{2}-y^2) + \frac{c}{3\sqrt{2}}(x-\sqrt{2}y)$	$(\delta m^{\mathrm{v}}_{s,08})^2$	$-\frac{N_c g^4}{8\sqrt{2}\pi^2}(\frac{1}{4}(x^2X-2y^2Y)+\frac{1}{3}(x^2-2y^2))$
$(m^{\mathrm{m}}_{\pi})^2$	$m^2 + \lambda_1(x^2+y^2) + \frac{\lambda_2}{2}x^2 - \frac{\sqrt{2}c}{2}y$	$(\delta m^{\mathrm{v}}_{p,11})^2$	$-\frac{N_c g^4}{64\pi^2}x^2X$
$(m^{\mathrm{m}}_{K})^2$	$m^2 + \lambda_1(x^2+y^2) + \frac{\lambda_2}{2}(x^2-\sqrt{2}xy+2y^2) - \frac{c}{2}x$	$(\delta m^{\mathrm{v}}_{p,44})^2$	$-\frac{N_c g^4}{64\pi^2}(\frac{x-\sqrt{2}y}{x^2-2y^2})(x^3X+2\sqrt{2}y^3Y)$
$(m^{\mathrm{m}}_{p,00})^2$	$m^2 + \lambda_1(x^2+y^2) + \frac{\lambda_2}{3}(x^2+y^2) + \frac{c}{3}(2x+\sqrt{2}y)$	$(\delta m^{\mathrm{v}}_{p,00})^2$	$-\frac{N_c g^4}{96\pi^2}(x^2X+y^2Y)$
$(m^{\mathrm{m}}_{p,88})^2$	$m^2 + \lambda_1(x^2+y^2) + \frac{\lambda_2}{6}(x^2+4y^2) - \frac{c}{6}(4x-\sqrt{2}y)$	$(\delta m^{\mathrm{v}}_{p,88})^2$	$-\frac{N_c g^4}{192\pi^2}(x^2X+4y^2Y)$
$(m^{\mathrm{m}}_{p,08})^2$	$\frac{\sqrt{2}\lambda_2}{6}(x^2-2y^2) - \frac{c}{6}(\sqrt{2}x-2y)$	$(\delta m^{\mathrm{v}}_{p,08})^2$	$-\frac{N_c g^4}{96\sqrt{2}\pi^2}(x^2X-2y^2Y)$

in Table IV for all the mesons of scalar and pseudoscalar nonets. The vacuum mass expressions $(m^{\mathrm{m}}_{\alpha,ab})^2$ for these mesons as originally evaluated from the second derivative of pure mesonic potential in Refs. [29,35] are also given in this table. Here, when $\alpha = \mathrm{s}$, the (11) element gives squared mass of the scalar a_0 meson, which is degenerate with the (22) and (33) elements. Similarly, the (44) element, which is degenerate with (55), (66), and (77) elements, gives the squared κ meson mass. The squared σ and f_0 meson masses are obtained by diagonalizing the scalar mass matrix in the (00)–(88) sector, and we get a scalar mixing angle θ_S. We have a completely analogous situation for the pseudoscalar sector ($\alpha = \mathrm{p}$) with the following identification: the (11) element gives the squared pion mass and the squared kaon mass is given by the (44) element. Further, the diagonalization of the (00)–(88) sector of the pseudoscalar mass matrix gives the squared masses of η and η', and analogously we get a pseudoscalar mixing angle θ_P.

In the QMVT/PQMVT model calculations, the vacuum mass expressions in Eq. (32) that determine λ_2 and c are $m_\pi^2 = (m^{\mathrm{m}}_\pi)^2 + (\delta m^{\mathrm{v}}_{p,11})^2$, $m_K^2 = (m^{\mathrm{m}}_K)^2 + (\delta m^{\mathrm{v}}_{p,44})^2$, and $m_\eta^2 + m_{\eta'}^2 = m_{p,00}^2 + m_{p,88}^2$, where $m_{p,00}^2 = (m^{\mathrm{m}}_{p,00})^2 + (\delta m^{\mathrm{v}}_{p,00})^2$ and $m_{p,88}^2 = (m^{\mathrm{m}}_{p,88})^2 + (\delta m^{\mathrm{v}}_{p,88})^2$. We can write $m_\eta^2 + m_{\eta'}^2 = (m^{\mathrm{m}}_\eta)^2 + (m^{\mathrm{m}}_{\eta'})^2 + (\delta m^{\mathrm{v}}_{p,00})^2 + (\delta m^{\mathrm{v}}_{p,88})^2$, where $(m^{\mathrm{m}}_\eta)^2 + (m^{\mathrm{m}}_{\eta'})^2 = (m^{\mathrm{m}}_{p,00})^2 + (m^{\mathrm{m}}_{p,88})^2$. Using mass modification expressions $(\delta m^{\mathrm{v}}_{\alpha,ab})^2$ given in Table IV, we write

$$
\begin{aligned}
(m^{\mathrm{m}}_K)^2 &= m_K^2 + \frac{N_c g^4}{64\pi^2}\left(\frac{x-\sqrt{2}y}{x^2-2y^2}\right)(x^3X + 2\sqrt{2}y^3Y),\\
(m^{\mathrm{m}}_\pi)^2 &= m_\pi^2 + \frac{N_c g^4}{64\pi^2}x^2X, \quad \text{and}\\
((m^{\mathrm{m}}_\eta)^2 + (m^{\mathrm{m}}_{\eta'})^2) &= (m_\eta^2 + m_{\eta'}^2) + \frac{N_c g^4}{192\pi^2}(3x^2X + 6y^2Y).
\end{aligned}
\tag{A2}
$$

The f_π and f_K give vacuum condensates according to the partially conserved axial vector current (PCAC) relation. The $\mathrm{x} = \sigma_x = f_\pi$ and $\mathrm{y} = \sigma_y = (\frac{2f_K - f_\pi}{\sqrt{2}})$ at $T = 0$. The parameters λ_2 and c in vacuum are obtained as

$$
\lambda_2 = \frac{3(2f_K - f_\pi)(m^{\mathrm{m}}_K)^2 - (2f_K + f_\pi)(m^{\mathrm{m}}_\pi)^2 - 2((m^{\mathrm{m}}_\eta)^2 + (m^{\mathrm{m}}_{\eta'})^2)(f_K - f_\pi)}{(3f_\pi^2 + 8f_K(f_K - f_\pi))(f_K - f_\pi)} \tag{A3}
$$

$$
c = \frac{(m^{\mathrm{m}}_K)^2 - (m^{\mathrm{m}}_\pi)^2}{f_K - f_\pi} - \lambda_2(2f_K - f_\pi). \tag{A4}
$$

When expressions of $(m^{\mathrm{m}}_\pi)^2$, $(m^{\mathrm{m}}_K)^2$, and $((m^{\mathrm{m}}_\eta)^2 + (m^{\mathrm{m}}_{\eta'})^2)$ from Eq. (A2) are substituted in Eqs. (A3) and (A4) and the vacuum value of the condensates are used, the final rearrangement of terms yields

TABLE V. The squared masses of scalar and pseudoscalar mesons that are obtained after the diagonalization of the 00–88 sector of the mass matrix. The meson masses in the nonstrange $\sigma_{NS}(\eta_{NS})$ and strange $\sigma_S(\eta_S)$ basis are given in the last two rows.

	Scalar Meson Masses		Pseudoscalar Meson Masses
m_σ^2	$m_{s,00}^2\cos^2\theta_s + m_{s,88}^2\sin^2\theta_s + 2m_{s,08}^2\sin\theta_s\cos\theta_s$	$m_{\eta'}^2$	$m_{p,00}^2\cos^2\theta_p + m_{p,88}^2\sin^2\theta_p + 2m_{p,08}^2\sin\theta_p\cos\theta_p$
$m_{f_0}^2$	$m_{s,00}^2\sin^2\theta_s + m_{s,88}^2\cos^2\theta_s - 2m_{s,08}^2\sin\theta_s\cos\theta_s$	m_η^2	$m_{p,00}^2\sin^2\theta_p + m_{p,88}^2\cos^2\theta_p - 2m_{p,08}^2\sin\theta_p\cos\theta_p$
$m_{\sigma_{NS}}^2$	$\frac{1}{3}(2m_{s,00}^2 + m_{s,88}^2 + 2\sqrt{2}m_{s,08}^2)$	$m_{\eta_{NS}}^2$	$\frac{1}{3}(2m_{p,00}^2 + m_{p,88}^2 + 2\sqrt{2}m_{p,08}^2)$
$m_{\sigma_S}^2$	$\frac{1}{3}(m_{s,00}^2 + 2m_{s,88}^2 - 2\sqrt{2}m_{s,08}^2)$	$m_{\eta_S}^2$	$\frac{1}{3}(m_{p,00}^2 + 2m_{p,88}^2 - 2\sqrt{2}m_{p,08}^2)$

$$\lambda_2 = \lambda_{2s} + n + \lambda_{2+} + \lambda_{2\mathrm{M}}, \quad \text{where } \lambda_{2s} = \frac{3(2f_K - f_\pi)m_K^2 - (2f_K + f_\pi)m_\pi^2 - 2(m_\eta^2 + m_{\eta'}^2)(f_K - f_\pi)}{(3f_\pi^2 + 8f_K(f_K - f_\pi))(f_K - f_\pi)},$$
$$n = \frac{N_c g^4}{32\pi^2}, \qquad \lambda_{2+} = \frac{nf_\pi^2}{f_K(f_K - f_\pi)}\log\left(\frac{2f_K - f_\pi}{f_\pi}\right) \text{ and scale-dependent part } \lambda_{2\mathrm{M}} = 4n\log\left(\frac{g(2f_K - f_\pi)}{2\mathrm{M}}\right) \tag{A5}$$

$$c = \frac{m_K^2 - m_\pi^2}{f_K - f_\pi} - \lambda_{2s}(2f_K - f_\pi). \tag{A6}$$

We note that the λ_{2s} is equal to the earlier λ_2 parameter determined in the QM/PQM model calculations in Refs. [29,35,44]. In the present calculation, the proper renormalization of fermionic vacuum leads to the augmentation of λ_{2s} by the addition of a term $(\mathrm{n} + \lambda_{2+})$, and further we get a renormalization scale M dependent contribution $\lambda_{2\mathrm{M}}$ in the expression of the λ_2 in Eq. (A5).

We get the complete cancelation of M dependence in the evaluation of c also and finally its value turns out to be the same as in the QM model. The scale M independent expression of m_π^2 obtained in Appendix B can be used with $\mathrm{x} = f_\pi$ and $\mathrm{y} = (\frac{2f_K - f_\pi}{\sqrt{2}})$ to express m^2 in terms of λ_1,

$$m^2 = m_\pi^2 - \lambda_1\left\{f_\pi^2 + \frac{(2f_K - f_\pi)^2}{2}\right\} - \frac{f_\pi^2}{2}\left[\lambda_{2\mathrm{v}} - 4n\log\left\{\frac{f_\pi}{(2f_K - f_\pi)}\right\}\right] + \frac{c}{2}(2f_K - f_\pi). \tag{A7}$$

When we use the formula of m_σ^2 in Table V of Appendix B (with the vacuum values of the masses $m_{s,00}^2$, $m_{s,88}^2$, $m_{s,08}^2$, and the mixing angle θ_S) and substitute the above expression of m^2 in it, we will get the numerical value of λ_1 for $m_\sigma = 600$ MeV, and we will put $m_\pi = 138$ MeV. The explicit symmetry-breaking parameters h_x and h_y do not change due to the fermionic vacuum correction.

APPENDIX B: SCALE INDEPENDENT MESON MASSES

When the value of λ_2 in Appendix A is substituted in the mass expressions $(m_{\alpha,ab}^{\mathrm{m}})^2$, the logarithmic M dependence of λ_2 neatly cancels with the scale dependence already existing in the mass modifications $(\delta m_{\alpha,ab}^{\mathrm{v}})^2$ due to the fermionic vacuum correction, and the final expressions of meson masses $m_{\alpha,ab}^2$ become free of any scale dependence when these two contributions are added together. The mixing angles obtained from these masses will naturally be independent of the renormalization scale. The expressions of the scale-independent meson masses are derived in the following:

Substituting the value of λ_2 from Eq. (A5) in the respective terms $(m_{a_0}^{\mathrm{m}})^2$, $(m_\kappa^{\mathrm{m}})^2$, $(m_{s,00}^{\mathrm{m}})^2$, $(m_{s,88}^{\mathrm{m}})^2$, and $(m_{s,08}^{\mathrm{m}})^2$ of the corresponding formulas $m_{a_0}^2 = (m_{a_0}^{\mathrm{m}})^2 + (\delta m_{s,11}^{\mathrm{v}})^2$, $m_\kappa^2 = (m_\kappa^{\mathrm{m}})^2 + (\delta m_{s,44}^{\mathrm{v}})^2$, $m_{s,00}^2 = (m_{s,00}^{\mathrm{m}})^2 + (\delta m_{s,00}^{\mathrm{v}})^2$, $m_{s,88}^2 = (m_{s,88}^{\mathrm{m}})^2 + (\delta m_{s,88}^{\mathrm{v}})^2$, and $m_{s,08}^2 = (m_{s,08}^{\mathrm{m}})^2 + (\delta m_{s,08}^{\mathrm{v}})^2$, we obtain the renormalization scale M independent mass formulas of all the mesons in the scalar nonet. We write $\lambda_{2\mathrm{v}}$ for $\lambda_{2s} + \lambda_{2+}$,

$$m_{a_0}^2 = m^2 + \lambda_1(x^2 + y^2) + \left[\lambda_{2s} + n + \lambda_{2+} + 4n\log\left\{\frac{g(2f_K - f_\pi)}{2\mathrm{M}}\right\}\right]\frac{3x^2}{2} + \frac{\sqrt{2}c}{2}y - n\left[4 + 3\left\{1 + 4\log\left(\frac{gx}{2\mathrm{M}}\right)\right\}\right]\frac{x^2}{2}$$
$$= m^2 + \lambda_1(x^2 + y^2) + \left[\lambda_{2\mathrm{v}} - 4n\log\left\{\frac{x}{(2f_K - f_\pi)}\right\} - \frac{4n}{3}\right]\frac{3x^2}{2} + \frac{\sqrt{2}c}{2}y. \tag{B1}$$

$$m_\kappa^2 = m^2 + \lambda_1(x^2+y^2) + \left[\lambda_{2s} + n + \lambda_{2+} + 4n\log\left\{\frac{g(2f_K - f_\pi)}{2\mathrm{M}}\right\}\right]\frac{(x^2+\sqrt{2}xy+2y^2)}{2} + \frac{c}{2}x$$
$$- \frac{n}{2}\left(\frac{x+\sqrt{2}y}{x^2-2y^2}\right)\left[x^3\left\{1+4\log\left(\frac{gx}{2\mathrm{M}}\right)\right\} - 2\sqrt{2}y^3\left\{1+4\log\left(\frac{gy}{\sqrt{2}\mathrm{M}}\right)\right\}\right]$$
$$= m^2 + \lambda_1(x^2+y^2) + \left[\lambda_{2\mathrm{v}} - 4n\log\left\{\frac{x}{(2f_K - f_\pi)}\right\}\right]\frac{(x^2+\sqrt{2}xy+2y^2)}{2} + \frac{c}{2}x + \frac{4\sqrt{2}ny^3}{(x-\sqrt{2}y)}\log\frac{\sqrt{2}y}{x}. \quad \text{(B2)}$$

$$m_{s,00}^2 = m^2 + \frac{\lambda_1}{3}(7x^2 + 4\sqrt{2}xy + 5y^2) + \left[\lambda_{2s} + n + \lambda_{2+} + 4n\log\left\{\frac{g(2f_K - f_\pi)}{2\mathrm{M}}\right\}\right](x^2+y^2) - \frac{\sqrt{2}c}{3}(\sqrt{2}x+y)$$
$$- \frac{n}{3}\left[3\left(x^2\left\{1+4\log\frac{gx}{2\mathrm{M}}\right\} + y^2\left\{1+4\log\frac{gy}{\sqrt{2}\mathrm{M}}\right\}\right) + 4(x^2+y^2)\right]$$
$$= m^2 + \frac{\lambda_1}{3}(7x^2 + 4\sqrt{2}xy + 5y^2) + \left(\lambda_{2\mathrm{v}} - \frac{4n}{3}\right)(x^2+y^2) - 4n\left[x^2\log\frac{x}{(2f_K - f_\pi)} + y^2\log\frac{\sqrt{2}y}{(2f_K - f_\pi)}\right]$$
$$- \frac{c(2x+\sqrt{2}y)}{3}. \quad \text{(B3)}$$

$$m_{s,88}^2 = m^2 + \frac{\lambda_1}{3}(5x^2 - 4\sqrt{2}xy + 7y^2) + \left[\lambda_{2s} + n + \lambda_{2+} + 4n\log\left\{\frac{g(2f_K - f_\pi)}{2\mathrm{M}}\right\}\right]\left(\frac{x^2}{2} + 2y^2\right) + \frac{\sqrt{2}c}{3}\left(\sqrt{2}x - \frac{y}{2}\right)$$
$$- \frac{n}{6}\left[3\left(x^2\left\{1+4\log\frac{gx}{2\mathrm{M}}\right\} + 4y^2\left\{1+4\log\frac{gy}{\sqrt{2}\mathrm{M}}\right\}\right) + 4(x^2+4y^2)\right]$$
$$= m^2 + \frac{\lambda_1}{3}(5x^2 - 4\sqrt{2}xy + 7y^2) + \left(\lambda_{2\mathrm{v}} - \frac{4n}{3}\right)\left(\frac{x^2}{2} + 2y^2\right) - 2n\left[x^2\log\frac{x}{(2f_K - f_\pi)} + 4y^2\log\frac{\sqrt{2}y}{(2f_K - f_\pi)}\right]$$
$$+ \frac{c(2x - \frac{y}{\sqrt{2}})}{3}. \quad \text{(B4)}$$

$$m_{s,08}^2 = 2\frac{\lambda_1}{3}(\sqrt{2}x^2 - xy - \sqrt{2}y^2) + \sqrt{2}\left[\lambda_{2s} + n + \lambda_{2+} + 4n\log\left\{\frac{g(2f_K - f_\pi)}{2\mathrm{M}}\right\}\right]\left(\frac{x^2}{2} - y^2\right) + \frac{c}{3\sqrt{2}}(x - \sqrt{2}y)$$
$$- \frac{n}{\sqrt{2}}\left[x^2\left\{1+4\log\frac{gx}{2\mathrm{M}}\right\} - 2y^2\left\{1+4\log\frac{gy}{\sqrt{2}\mathrm{M}}\right\} + \frac{4}{3}(x^2-2y^2)\right]$$
$$= 2\frac{\lambda_1}{3}(\sqrt{2}x^2 - xy - \sqrt{2}y^2) + \sqrt{2}\left(\lambda_{2\mathrm{v}} - \frac{4n}{3}\right)\left(\frac{x^2}{2} - y^2\right) - 2\sqrt{2}n\left[x^2\log\frac{x}{(2f_K - f_\pi)} - 2y^2\log\frac{\sqrt{2}y}{(2f_K - f_\pi)}\right]$$
$$+ \frac{c(x - \sqrt{2}y)}{3\sqrt{2}}. \quad \text{(B5)}$$

Substituting the value of λ_2 from Eq. (A5) in the respective expressions of $(m_\pi^{\mathrm{m}})^2$, $(m_K^{\mathrm{m}})^2$, $(m_{p,00}^{\mathrm{m}})^2$, $(m_{p,88}^{\mathrm{m}})^2$, and $(m_{p,08}^{\mathrm{m}})^2$ in the corresponding formulas $m_\pi^2 = (m_\pi^{\mathrm{m}})^2 + (\delta m_{p,11}^{\mathrm{v}})^2$, $m_K^2 = (m_K^{\mathrm{m}})^2 + (\delta m_{p,44}^{\mathrm{v}})^2$, $m_{p,00}^2 = (m_{p,00}^{\mathrm{m}})^2 + (\delta m_{p,00}^{\mathrm{v}})^2$, $m_{p,88}^2 = (m_{p,88}^{\mathrm{m}})^2 + (\delta m_{p,88}^{\mathrm{v}})^2$, and $m_{p,08}^2 = (m_{p,08}^{\mathrm{m}})^2 + (\delta m_{p,08}^{\mathrm{v}})^2$, we obtain the following renormalization scale M independent mass formulas for the pseudoscalar mesons:

$$m_\pi^2 = m^2 + \lambda_1(x^2+y^2) + \left[\lambda_{2s} + n + \lambda_{2+} + 4n\log\left\{\frac{g(2f_K - f_\pi)}{2\mathrm{M}}\right\}\right]\frac{x^2}{2} - \frac{\sqrt{2}c}{2}y - n\left[1+4\log\left(\frac{gx}{2\mathrm{M}}\right)\right]\frac{x^2}{2}$$
$$= m^2 + \lambda_1(x^2+y^2) + \left[\lambda_{2\mathrm{v}} - 4n\log\left\{\frac{x}{(2f_K - f_\pi)}\right\}\right]\frac{x^2}{2} - \frac{\sqrt{2}c}{2}y, \quad \text{(B6)}$$

$$m_K^2 = m^2 + \lambda_1(x^2+y^2) + \left[\lambda_{2s} + n + \lambda_{2+} + 4n\log\left\{\frac{g(2f_K - f_\pi)}{2\mathrm{M}}\right\}\right]\frac{(x^2 - \sqrt{2}xy + 2y^2)}{2} - \frac{c}{2}x$$
$$- \frac{n}{2}\left(\frac{x-\sqrt{2}y}{x^2-2y^2}\right)\left[x^3\left\{1 + 4\log\left(\frac{gx}{2\mathrm{M}}\right)\right\} + 2\sqrt{2}y^3\left\{1 + 4\log\left(\frac{gy}{\sqrt{2}\mathrm{M}}\right)\right\}\right]$$
$$= m^2 + \lambda_1(x^2+y^2) + \left[\lambda_{2\mathrm{v}} - 4n\log\left\{\frac{x}{(2f_K - f_\pi)}\right\}\right]\frac{(x^2 - \sqrt{2}xy + 2y^2)}{2} - \frac{c}{2}x - \frac{4\sqrt{2}ny^3}{(x+\sqrt{2}y)}\log\frac{\sqrt{2}y}{x}, \quad \text{(B7)}$$

$$m_{p,00}^2 = m^2 + \lambda_1(x^2+y^2) + \left[\lambda_{2s} + n + \lambda_{2+} + 4n\log\left\{\frac{g(2f_K - f_\pi)}{2\mathrm{M}}\right\}\right]\frac{(x^2+y^2)}{3} + \frac{\sqrt{2}c}{3}(\sqrt{2}x + y)$$
$$- \frac{n}{3}\left[x^2\left(1 + 4\log\frac{gx}{2\mathrm{M}}\right) + y^2\left(1 + 4\log\frac{gy}{\sqrt{2}\mathrm{M}}\right)\right]$$
$$= m^2 + \lambda_1(x^2+y^2) + \frac{\lambda_{2\mathrm{v}}}{3}(x^2+y^2) - \frac{4n}{3}\left[x^2\log\frac{x}{(2f_K - f_\pi)} + y^2\log\frac{\sqrt{2}y}{(2f_K - f_\pi)}\right] + \frac{c(2x+\sqrt{2}y)}{3}, \quad \text{(B8)}$$

$$m_{p,88}^2 = m^2 + \lambda_1(x^2+y^2) + \left[\lambda_{2s} + n + \lambda_{2+} + 4n\log\left\{\frac{g(2f_K - f_\pi)}{2\mathrm{M}}\right\}\right]\frac{(x^2+4y^2)}{6} - \frac{\sqrt{2}c}{3}\left(\sqrt{2}x - \frac{y}{2}\right)$$
$$- \frac{n}{6}\left[x^2\left(1 + 4\log\frac{gx}{2\mathrm{M}}\right) + 4y^2\left(1 + 4\log\frac{gy}{\sqrt{2}\mathrm{M}}\right)\right]$$
$$= m^2 + \lambda_1(x^2+y^2) + \frac{\lambda_{2\mathrm{v}}}{6}(x^2+4y^2) - \frac{2n}{3}\left[x^2\log\frac{x}{(2f_K - f_\pi)} + 4y^2\log\frac{\sqrt{2}y}{(2f_K - f_\pi)}\right] - \frac{c(2x - \frac{y}{\sqrt{2}})}{3}, \quad \text{(B9)}$$

$$m_{p,08}^2 = \frac{\sqrt{2}}{6}\left[\lambda_{2s} + n + \lambda_{2+} + 4n\log\left\{\frac{g(2f_K - f_\pi)}{2\mathrm{M}}\right\}\right](x^2 - 2y^2) - \frac{c}{6}(\sqrt{2}x - 2y)$$
$$- \frac{n}{3\sqrt{2}}\left[x^2\left(1 + 4\log\frac{gx}{2\mathrm{M}}\right) - 2y^2\left(1 + 4\log\frac{gy}{\sqrt{2}\mathrm{M}}\right)\right]$$
$$= \frac{\sqrt{2}\lambda_{2\mathrm{v}}}{6}(x^2 - 2y^2) - \frac{2\sqrt{2}n}{3}\left[x^2\log\frac{x}{(2f_K - f_\pi)} - 2y^2\log\frac{\sqrt{2}y}{(2f_K - f_\pi)}\right] - \frac{c(\sqrt{2}x - 2y)}{6}. \quad \text{(B10)}$$

[1] E. V. Shuryak, Phys. Rep. **61**, 71 (1980); **115**, 151 (1984).
[2] J. Rafelski, Phys. Rep. **88**, 331 (1982); **142**, 167 (1986).
[3] L. D. McLerran and B. Svetitsky, Phys. Rev. D**24**, 450 (1981); B. Svetitsky, Phys. Rep. **132**, 1 (1986).
[4] B. Muller, Rep. Prog. Phys. **58**, 611 (1995).
[5] H. Meyer-Ortmanns, Rev. Mod. Phys. **68**, 473 (1996).
[6] D. H. Rischke, Prog. Part. Nucl. Phys. **52**, 197 (2004).
[7] A. M. Polyakov, Phys. Lett. **72B**, 477 (1978).
[8] R. D. Pisarski, Phys. Rev. D **62**, 111501(R) (2000).
[9] B. Layek, A. P. Mishra, A. M. Srivastava, and V. K. Tiwari, Phys. Rev. D **73**, 103514 (2006).
[10] O. Kaczmarek, F. Karsch, P. Petreczky, and F. Zantow, Phys. Lett. B **543**, 41 (2002).
[11] F. Karsch, Lect. Notes Phys. **583**, 209 (2002).
[12] Z. Fodor, S. D. Katz, and K. K. Szabo, Phys. Lett. B **568**, 73 (2003).
[13] C. R. Allton, M. Doring, S. Ejiri, S. J. Hands, O. Kaczmarek, F. Karsch, E. Laermann, and K. Redlich, Phys. Rev. D **71**, 054508 (2005).
[14] F. Karsch, J. Phys. G **31**, S633 (2005).
[15] F. Karsch, J. Phys. G **34**, S627 (2007).
[16] Y. Aoki, Z. Fodor, S. D. Katz, and K. K. Szabo, Phys. Lett. B **643**, 46 (2006).
[17] Y. Aoki, G. Endrodi, Z. Fodor, S. D. Katz, and K. K. Szabo, Nature (London) **443**, 675 (2006).
[18] S. Borsanyi, G. Endrodi, Z. Fodor, A. Jakovac, S. D. Katz, S. Krieg, C. Ratti, and K. K. Szabo, arXiv:1011.4229.
[19] C. Schmidt (HotQCD Collaboration), AIP Conf. Proc. **1343**, 513 (2011).
[20] M. Cheng, N. H. Christ, S. Datta, J. van der Heide, C. Jung, F. Karsch, O. Kaczmarek, E. Laermann *et al.*, Phys. Rev. D **77**, 014511 (2008).

[21] A. Bazavov, T. Bhattacharya, M. Cheng, N. H. Christ, C. DeTar, S. Ejiri, S. Gottlieb, R. Gupta *et al.*, Phys. Rev. D **80**, 014504 (2009).

[22] S. Borsanyi, G. Endrodi, Z. Fodor, A. Jakovac, S. D. Katz, S. Krieg, C. Ratti, and K. K. Szabo, J. High Energy Phys. 11 (2010) 077.

[23] S. Borsanyi, Z. Fodor, C. Hoelbling, S. D. Katz, S. Krieg, C. Ratti, and K. K. Szabo, J. High Energy Phys. 09 (2010) 073.

[24] S. Borsanyi, G. Endrodi, Z. Fodor, C. Hoelbling, S. D. Katz, S. Krieg, C. Ratti, and K. K. Szabo, Acta Phys. Pol. B Proc. Suppl. **4**, 593 (2011).

[25] A. Bazavov, T. Bhattacharya, M. Cheng, C. DeTar, H. T. Ding, S. Gottlieb, R. Gupta, P. Hegde *et al.*, Phys. Rev. D **85**, 054503 (2012).

[26] R. D. Pisarski and F. Wilczek, Phys. Rev. D **29**, 338 (1984).

[27] S. Chiku and T. Hatsuda, Phys. Rev. D **58**, 076001 (1998).

[28] J. Schaffner-Bielich, Phys. Rev. Lett. **84**, 3261 (2000).

[29] J. T. Lenaghan, D. H. Rischke, and J. Schaffner-Bielich, Phys. Rev. D **62**, 085008 (2000).

[30] O. Scavenius, A. Mocsy, I. N. Mishustin, and D. H. Rischke, Phys. Rev. C **64**, 045202 (2001).

[31] T. Herpay, A. Patkós, Zs. Szép, and P. Szépfalusy, Phys. Rev. D **71**, 125017 (2005).

[32] T. Herpay and Zs. Szép, Phys. Rev. D **74**, 025008 (2006).

[33] P. Kovács and Zs. Szép, Phys. Rev. D **75**, 025015 (2007).

[34] B. J. Schaefer and J. Wambach, Phys. Rev. D **75**, 085015 (2007).

[35] B. J. Schaefer and M. Wagner, Phys. Rev. D **79**, 014018 (2009).

[36] B. J. Schaefer and M. Wagner, Prog. Part. Nucl. Phys. **62**, 381 (2009).

[37] E. S. Bowman and J. I. Kapusta, Phys. Rev. C **79**, 015202 (2009); J. I. Kapusta and E. S. Bowman, Nucl. Phys. **A830**, 721c (2009).

[38] L. Ferroni, V. Koch, and M. B. Pinto, Phys. Rev. C **82**, 055205 (2010).

[39] R. Khan, and L. T. Kyllingstad, AIP Conf. Proc. **1343**, 504 (2011); J. O. Andersen, R. Khan, and L. T. Kyllingstad, arXiv:1102.2779.

[40] G. Fejos and A. Patkos, Phys. Rev. D **82**, 045011 (2010); **85**, 117502 (2012).

[41] G. Fejos, Phys. Rev. D **87**, 056006 (2013).

[42] B. J. Schaefer, J. M. Pawlowski, and J. Wambach, Phys. Rev. D **76**, 074023 (2007).

[43] J. Braun and H. Gies, Phys. Lett. B **645**, 53 (2007); J. High Energy Phys. 06 (2006) 024.

[44] U. S. Gupta and V. K. Tiwari, Phys. Rev. D **81**, 054019 (2010).

[45] B. J. Schaefer, M. Wagner, and J. Wambach, Phys. Rev. D **81**, 074013 (2010).

[46] B. J. Schaefer, M. Wagner, and J. Wambach, Proc. Sci., CPOD (2009) 017.

[47] H. Mao, J. Jin, and M. Huang, J. Phys. G **37**, 035001 (2010).

[48] T. K. Herbst, J. M. Pawlowski, and B.-J. Schaefer, Phys. Lett. B **696**, 58 (2011).

[49] B.-J. Schaefer, arXiv:1102.2772; J. M. Pawlowski, AIP Conf. Proc. **1343**, 75 (2011).

[50] G. Marko and Zs. Szep, Phys. Rev. D **82**, 065021 (2010).

[51] T. Kahara and K. Tuominen, Phys. Rev. D **78**, 034015 (2008); **80**, 114022 (2009); **82**, 114026 (2010).

[52] S. Digal, E. Laermann, and H. Satz, Eur. Phys. J. C **18**, 583 (2001).

[53] C. Ratti, M. A. Thaler, and W. Weise, Phys. Rev. D **73**, 014019 (2006).

[54] S. Rößner, C. Ratti, and W. Weise, Phys. Rev. D **75**, 034007 (2007).

[55] H. Hansen, W. M. Alberico, A. Beraudo, A. Molinari, M. Nardi, and C. Ratti, Phys. Rev. D **75**, 065004 (2007).

[56] S. Rößner, T. Hell, C. Ratti, and W. Weise, Nucl. Phys. **A814**, 118 (2008).

[57] S. K. Ghosh, T. K. Mukherjee, M. G. Mustafa, and R. Ray, Phys. Rev. D **73**, 114007 (2006).

[58] C. Sasaki, B. Friman, and K. Redlich, Phys. Rev. D **75**, 074013 (2007).

[59] T. Hell, S. Rößner, M. Cristoforetti, and W. Weise, Phys. Rev. D **79**, 014022 (2009).

[60] H. Abuki, R. Anglani, R. Gatto, G. Nardulli, and M. Ruggieri, Phys. Rev. D **78**, 034034 (2008).

[61] M. Ciminale, R. Gatto, N. D. Ippolito, G. Nardulli, and M. Ruggieri, Phys. Rev. D **77**, 054023 (2008).

[62] W.-J. Fu, Z. Zhang, and Y.-X. Liu, Phys. Rev. D **77**, 014006 (2008).

[63] K. Fukushima, Phys. Lett. B **591**, 277 (2004).

[64] K. Fukushima, Phys. Rev. D **77**, 114028 (2008).

[65] K. Fukushima, Phys. Rev. D **78**, 114019 (2008).

[66] K. Fukushima, Phys. Rev. D **79**, 074015 (2009).

[67] G. A. Contrera, M. Orsaria, and N. N. Scoccola, Phys. Rev. D **82**, 054026 (2010).

[68] A. E. Radzhabov, D. Blaschke, M. Buballa, and M. K. Volkov, Phys. Rev. D **83**, 116004 (2011).

[69] O. Lourenco, M. Dutra, T. Frederico, A. Delfino, and M. Malheiro, Phys. Rev. D **85**, 097504 (2012); O. Lourenco, M. Dutra, A. Delfino, and M. Malheiro, Phys. Rev. D **84**, 125034 (2011).

[70] H. Hansen, W. M. Alberico, A. Beraudo, A. Molinari, M. Nardi, and C. Ratti, Phys. Rev. D **75**, 065004 (2007).

[71] P. Costa, M. C. Ruivo, C. A. de Sousa, and Yu. L. Kalinovsky, Phys. Rev. D **70**, 116013 (2004).

[72] P. Costa, M. C. Ruivo, C. A. de Sousa, and Yu. L. Kalinovsky, Phys. Rev. D **71**, 116002 (2005).

[73] P. Costa, M. C. Ruivo, C. A. de Sousa, H. Hansen, and W. M. Alberico, Phys. Rev. D **79**, 116003 (2009).

[74] G. A. Contrera, D. Gomez Dumm, and N. N. Scoccola, Phys. Rev. D **81**, 054005 (2010).

[75] A. A. Asipov, B. Hiller, and J. Da Providencia, Phys. Lett. B **634**, 48 (2006); A. A. Asipov, B. Hiller, A. H. Blin, and J. Da Providencia, Ann. Phys. (Amsterdam) **322**, 2021 (2007); A. A. Asipov, B. Hiller, J. Moreira, A. H. Blin, and J. Da Providencia, Phys. Lett. B **646**, 91 (2007); A. A. Asipov, B. Hiller, J. Moreira, and A. H. Blin, Phys. Lett. B **659**, 270 (2008); B. Hiller, J. Moreira, A. A. Asipov, and A. H. Blin, Acta Phys. Pol. B Proc. Suppl. **5**, 1171 (2012).

[76] G. 't Hooft, Phys. Rev. Lett. **37**, 8 (1976); Phys. Rev. D **14**, 3432 (1976).

[77] K. Fukushima, K. Ohnishi, and K. Ohta, Phys. Rev. C **63**, 045203 (2001).
[78] V. Skokov, B. Friman, E. Nakano, K. Redlich, and B.-J. Schaefer, Phys. Rev. D **82**, 034029 (2010).
[79] A. J. Mizher, M. N. Chernodub, and E. S. Fraga, Phys. Rev. D **82**, 105016 (2010).
[80] L. F. Palhares and E. S. Fraga, Phys. Rev. D **78**, 025013 (2008).
[81] E. S. Fraga, L. F. Palhares, and M. B. Pinto, Phys. Rev. D **79**, 065026 (2009).
[82] L. F. Palhares and E. S. Fraga, Phys. Rev. D **82**, 125018 (2010).
[83] U. S. Gupta and V. K. Tiwari, Phys. Rev. D **85**, 014010 (2012).
[84] B.-J. Schaefer and M. Wagner, Phys. Rev. D **85**, 034027 (2012).
[85] S. Chatterjee and K. A. Mohan, Phys. Rev. D **85**, 074018 (2012); **86**, 114021 (2012).
[86] V. K. Tiwari, Phys. Rev. D **86**, 094032 (2012).
[87] S. Weinberg, Phys. Rev. D **11**, 3583 (1975).
[88] J. I. Kapusta and C. Gale, *Finite Temperature Field Theory Principles and Applications* (Cambridge University Press, Cambridge, England, 2006).
[89] M. Quiros, in *Proceedings of The Summer School in High Energy Physics and Cosmology, ICTP Series in Theoretical Physics, Trieste, Italy, 1998*, edited by A. Masiero, G. Senjanovic, and A. Smirnov (World Scientific, Singapore, 1999), Vol. 15, p. 436.
[90] A. Bazavov and B. A. Berg, Phys. Rev. D **76**, 014502 (2007).